Regulation of invasion-associated actin dynamics by the *Chlamydia trachomatis* effectors TarP and TmeA

Matthew D. Romero and Rey A. Carabeo[1]

Department of Pathology and Microbiology, College of Medicine, University of Nebraska Medical Center, Omaha, NE

[1]Corresponding Author:
Department of Pathology and Microbiology
University of Nebraska Medical Center
985900 Nebraska Medical Center, Omaha, NE
Email: rey.carabeo@unmc.edu

Abstract:

The obligate intracellular pathogen *Chlamydia trachomatis* manipulates the host actin cytoskeleton to assemble actin-rich structures that drive pathogen entry. This actin remodeling event exhibits relatively rapid dynamics that, through quantitative live-cell imaging, was revealed to consist of three phases – a fast recruitment phase which abruptly transitions to a fast turnover phase before resolving into a slow turnover of actin, indicating the end of actin remodeling. Here, we investigate *Chlamydia* invasion in the context of actin dynamics. Efficient invasion was associated with robust actin remodeling kinetics, which was linked to signaling from the type-III secreted effectors TarP and TmeA, and the actin nucleating activities of formin 1 (Fmn1) and Arp2/3. Stable recruitment of Fmn1 and Arp2/3 was dependent upon TarP and/or TmeA, although TarP signaling was responsible for the majority of Fmn1 and Arp2/3 recruitment. Rapid actin kinetics were due in part to a collaborative functional interaction between two different classes of actin nucleators – formins, including formin 1 and the diaphanous-related formins mDia1 and mDia2, and the Arp2/3 complex. Inhibition of either formin or Arp2/3, or deletion of TarP and TmeA, prevented this collaboration and resulted in attenuated actin kinetics and invasion efficiency. Collectively, these data support a model wherein TarP and TmeA signaling are core components of actin remodeling that operate via stable recruitment of formin and Arp2/3. At the population level, the kinetics of recruitment and turnover of actin and its nucleators were linked. However, reanalysis of the data at the level of individual elementary bodies showed significant variation and a lack of correlation between the kinetics of recruitment and turnover, suggesting that accessory factors variably modify actin kinetics at individual entry sites. In summary, efficient chlamydial invasion is an effector-driven process that requires a specific profile of actin recruitment which arises following collaboration between formin and Arp2/3.

39 **Short Title: TarP and TmeA coordinate collaboration between Formin 1 and Arp2/3 during invasion**

40

41 **Author Summary:**

42 The obligate intracellular pathogen *Chlamydia trachomatis* relies upon manipulation of the host actin
43 cytoskeleton to drive its entry into host cells, such that impairment of actin dynamics
44 attenuates *Chlamydia* invasion. Collaboration between two classes of actin nucleators, formin and
45 Arp2/3, are known to enhance actin recruitment and turnover; we found that stable recruitment of both
46 proteins to the signaling complex established by the type III secreted effectors, TarP and TmeA, were
47 important for pathogen internalization. Furthermore, Formin 1 and Arp2/3 are co-recruited to sites of
48 entry, and pharmacological inhibition of either actin nucleator impaired recruitment of the other,
49 indicating a functional cooperation between branched and filamentous actin nucleation within pathogen
50 entry sites. Disruption of this cooperation negatively impacted both actin dynamics
51 and *Chlamydia* internalization, indicating that TarP- and TmeA-dependent entry of *Chlamydia* into non-
52 phagocytic cells operates through the recruitment and activation of Arp2/3 and Formin 1. Finally, kinetic
53 analysis of actin recruitment and turnover revealed that these processes were independently regulated,
54 in addition to implicating the presence of local factors that fine-tune actin dynamics and subsequent
55 invasion.

56

57 **Introduction**

58 Infections caused by the obligate intracellular bacterium *Chlamydia trachomatis* are both the leading
59 cause of preventable blindness and the most prevalent bacterial form of sexually transmitted disease
60 worldwide [1]. *Chlamydiae* feature a biphasic developmental cycle divided between metabolically inactive
61 elementary bodies, which infect host cells, and metabolically active reticulate bodies, which replicate in a
62 membrane-bound vacuole known as an inclusion [2]. Invading elementary bodies initially form a
63 reversible electrostatic attachment onto heparin sulfate proteoglycans on the host cell surface [3,4].
64 Shortly after, *Chlamydia* engages and activates a multitude of host cell receptors while simultaneously
65 delivering an array of bacterial effectors by a type III secretion system [5–7]. Activation of host receptors
66 and delivery of bacterial effectors during invasion allow *Chlamydia* to exploit regulatory components of
67 the actin cytoskeleton like Arp2/3, Rho GTPases, and vinculin amongst others [5,7–11]. By manipulating
68 cytoskeletal regulators, *Chlamydia* induces the formation of actin-rich microstructures on the cell surface
69 that facilitate engulfment of the pathogen [12,13]. These structures can adopt a variety of configurations,
70 including phagocytic cups, membrane ruffles, filopodia, and hypertrophic microvilli [9,14]. A distinguishing
71 characteristic of structures generated by *Chlamydia* during invasion is their rapid and highly localized
72 assembly [12]. Whereas *S. typhimurium* and *R. parkeri* recruit actin in a diffuse pattern over the span of
73 5-15 minutes [15–17], actin recruitment and localized assembly of invasion-associated structures by
74 *Chlamydia* is completed within two minutes [18].

75 Actin polymerization at the invasion site occurs is due in large part to the secretion of the bacterial
76 effectors TarP and TmeA, which jointly coordinate the assembly of a robust actin remodeling network at
77 *Chlamydia* entry sites. TarP and TmeA accomplish this task in part by their shared ability to recruit the
78 actin nucleator Arp2/3 during invasion. Arp2/3 is a complex of proteins which, upon activation, enhances
79 the rate of actin polymerization by nucleating branched actin filaments along a pre-existing "mother"
80 filament [19,20], and the resulting branched network in turn increases the number of sites for Arp2/3

81 binding and branched nucleation [21]. TarP and TmeA activate the Arp2/3 complex via downstream
82 activation of the nucleation promoting factors WAVE2 and N-WASP, respectively [9,22–24]. Signaling
83 through WAVE2 and N-WASP have each been shown to be important for *Chlamydia* engulfment, as
84 targeted disruption of either protein attenuated pathogen uptake [9,23,24]. Furthermore, siRNA
85 knockdown of WAVE2 prevented the recruitment of actin at entry sites, highlighting the importance of
86 Arp2/3 activation and subsequent actin remodeling in *Chlamydia* pathogenesis [9].

87 The actin remodeling network generated by *Chlamydia* enable the assembly of invasion-
88 associated structures which are comprised entirely or in part by elongated bundles of filamentous actin.
89 A class of actin nucleators known as formins participate in the assembly of actin-rich structures by
90 facilitating rapid incorporation of actin monomers onto the barbed end of actin filaments [25]. In turn,
91 these rapidly elongating filaments provide a highly localized protrusive force that gives rise to actin-rich
92 structures such as filopodia and microvilli [26–28]. Broadly, formins can be divided into two subclasses:
93 diaphanous-related formins (DRFs), which must be activated by Rho-GTPases before they can serve as
94 actin nucleators, and non-DRF formins, which do not require activation to participate in actin filament
95 elongation [29]. Once activated, formins dimerize and incorporate monomeric actin onto the barbed end
96 of an actin filament. Formins have been demonstrated to participate in the invasion of bacterial pathogens
97 including *L. monocytogenes*, *S. typhimurium*, and *B. burgdorferi* [30–32]. Likewise, invading *C. trachomatis*
98 is known to interact with hypertrophic microvillar structures that are enriched with filamentous actin [12],
99 raising the possibility that *Chlamydia* also utilizes formins during invasion.

100 The actin elongating properties of formins are known to synergize with the actin branching activity
101 of Arp2/3, generating a dense network of branched and elongated actin filaments [33]. This collaborative
102 interaction is essential for many cellular processes like cell motility, division, and phagocytosis [34,35],
103 and also enhances the actin remodeling capabilities of invading pathogens. For instance, the spiraling
104 filamentous protrusions formed by *B. burgdorferi* or the raised actin-rich pedestals of enteropathogenic

105 *E. coli* are both formed by collaboration between Arp2/3 and formin [36,37]. These pathogen-associated
106 structures are reminiscent of the structures generated during *C. trachomatis* invasion, introducing the
107 possibility that formin and Arp2/3 also act collaboratively during invasion to engulf the pathogen.

108 In addition to the multitude of proteins which regulate the polymerization of the actin
109 cytoskeleton, a handful of other proteins coordinate the depolymerization of actin [38]. Typically, actin
110 depolymerization factors target older actin filaments to generate monomeric actin, which in turn is
111 utilized to generate new actin filaments [39]. Despite their role in maintaining actin homeostasis, the
112 activities of host actin depolymerization factors are often counteracted by bacterial pathogens [40]. For
113 instance, the *C. pneumoniae* TarP ortholog CPN0572 displaces the actin depolymerization factor
114 ADF/cofilin to stabilize actin filaments during its invasion [41]. However, it is evident that actin turnover
115 is necessary for *Chlamydia* internalization, as treatment with the actin stabilizing compound jasplakinolide
116 prevents invasion [42]. Furthermore, actin recruitment observed in previous studies is highly transient
117 [18], indicating that *Chlamydia* employs a mechanism that induces a shift from the recruitment and
118 polymerization of actin toward an equally rapid depolymerization, which removes the dense network of
119 filaments generated by *Chlamydia* during invasion. The details regarding how *Chlamydia* accomplishes
120 actin depolymerization, or the signals that initiate this process remain unknown.

121 Given the importance of actin recruitment and turnover to chlamydial invasion, we investigated
122 this process by quantifying the relative contribution of TarP and TmeA to the overall actin dynamics during
123 invasion. Actin dynamics associated with efficient invasion consists of three phases: rapid recruitment, a
124 brief fast turnover phase, and a lingering slow turnover phase. We observed that *Chlamydia* strains lacking
125 either TarP or TmeA invaded epithelial cells less efficiently and exhibited altered actin dynamics; direct
126 comparison of the two mutants revealed a greater defect in actin dynamics in the TarP knockout strain.
127 The two mutants also exhibited quantifiable reduction in the recruitment and turnover kinetics for Arp2/3
128 and formin 1 (Fmn1), thus accounting for the significant differences in actin dynamics and subsequent

129 invasion. Using target-specific pharmacological inhibitors that affected actin nucleation, but not
130 association with nucleation promoting factors and/or actin filaments, we were able to demonstrate the
131 mutual recruitment of Arp2/3 and Fmn1 in an actin polymerization-dependent manner. Inhibition of one
132 was sufficient to inhibit recruitment of the other, indicating that their presence at the sites of invasion
133 was due to their respective abilities to bind and nucleate filamentous actin. Collectively analyzing
134 dynamics data for actin, Arp3, and Fmn1 at the single-elementary body level also showed that recruitment
135 and turnover rates were not strictly interdependent, hinting at additional molecular determinants of
136 invasion efficiency. In summary, this report established a functional hierarchy of TarP and TmeA which
137 operates to regulate actin dynamics, an observation that was not readily apparent from invasion efficiency
138 quantification alone. As such, we conclude that the rapid and highly localized actin network generated by
139 *Chlamydia* during invasion emerges as a consequence of collaboration between the activities of Arp2/3
140 and formin following their recruitment by TarP and TmeA.
141
142 **Results**
143 **Both TarP and TmeA are necessary for efficient invasion and optimal actin kinetics.**
144 Rapid and robust recruitment of actin is a hallmark of *Chlamydia* invasion, which is coordinated in part by
145 the secreted effectors TarP and TmeA via their ability to recruit actin modulatory proteins during invasion.
146 Recently, it was shown that TarP and TmeA synergistically enhance the in-vitro rate of actin
147 polymerization [24]. Genetic deletion of TarP (ΔTarP) or TmeA (ΔTmeA) attenuates pathogen entry, which
148 was rescued by cis-complementation of *ct456*/*tarp* (*cis*-TarP) or *ct694*/*tmea* (*cis*-TmeA). On the basis of
149 these observations, it was proposed that synergy between TmeA and TarP is an important determinant
150 of both robust actin kinetics and efficient invasion. To evaluate this claim, we quantified the rate and
151 intensity of actin recruitment at the entry sites of wild-type, single-knockout (ΔTarP, ΔTmeA), cis-
152 complemented (*cis*-TarP, *cis*-TmeA), or double-knockout (ΔTmeA/ΔTarP) *Chlamydia* strains (Fig. 1, Video

153 S1). Comparisons of actin recruitment between strains were derived by calculating their respective fold
154 recruitment values, which measures the fold increase of fluorescence intensity relative to the immediate
155 background. A detailed account of this process can be found in the supplementary data (Fig. S1). While all
156 strains retained the ability to recruit actin, we noted that the intensity of actin recruitment was diminished
157 upon deletion of TarP and/or TmeA (Fig. 1A,B). Wild-type and cis-complemented strains of *Chlamydia*
158 recruited actin at an average intensity of 18-fold above background, which was reduced by 5-fold
159 following TmeA deletion and 12-fold following TarP deletion. Interestingly, the peak intensity of actin
160 recruitment at ΔTmeA/ΔTarP entry sites (4.86 fold +/- 0.68) was only marginally reduced relative to ΔTarP
161 (6.27 fold +/- 1.10), suggesting that TmeA signaling alone is insufficient to generate robust actin kinetics
162 and that TarP accounts for the majority of the actin signal intensity during invasion. Despite this, and in
163 agreement with earlier studies, we found that deletion of either TmeA or TarP significantly reduced the
164 efficiency of *Chlamydia* internalization (Wild-type=76.2%, ΔTmeA=50.4%, ΔTarP=42.1%), and that
165 deletion of both effectors worsened this defect (ΔTmeA/ΔTarP=29.6%) (Fig. 1C). Collectively, these data
166 indicate that strains lacking TarP and/or TmeA are deficient in actin recruitment, which is linked to poor
167 invasion efficiency relative to either wild-type or *cis*-complemented strains.
168
169 **Recruitment and turnover of actin are slowed by deletion of TarP and/or TmeA**
170 In addition to reducing the intensity of actin recruitment, we also noted that the overall actin recruitment
171 profiles of ΔTarP and ΔTmeA strains differed from wild-type *Chlamydia*. In particular, both ΔTarP and
172 ΔTmeA/ΔTarP exhibit atypically transient actin recruitment, while ΔTmeA produces an intermediate
173 profile with slightly lower intensity and duration (Fig. 1B). These observations, coupled with reduced
174 invasion efficiency following TarP or TmeA deletion (Fig. 1C), indicate a link between actin kinetics and
175 invasion efficiency. We observed that the recruitment profile of actin exhibited three distinct phases: i)
176 recruitment, in which actin rapidly accumulates, ii) fast turnover, in which actin is rapidly lost from the

177 sites of invasion, likely through depolymerization and iii) slow turnover, in which actin is gradually
178 depolymerized over an extended time period (Fig. 1B). The entry and exit points for each phase were
179 determined by plotting the first derivative values corresponding to the velocity of recruitment and
180 turnover for each timepoint and is discussed in greater detail in the supplemental data (Fig. S2).

181 To compare the kinetics of actin recruitment and turnover between conditions, we employed
182 linear regression to calculate the slope, representing the rate of recruitment and turnover for each
183 recruitment event (Fig. S2,3), and mapped these values onto a violin plot to visualize the distribution of
184 rates for each strain (Fig. 1D,E, Table S1). Although wild-type and *cis*-TarP strains exhibited comparably
185 rapid actin recruitment (WT=0.287 fold/sec, *cis*-TarP=0.233 fold/sec), we observed a slower rate of actin
186 recruitment in cis-TmeA (0.178 fold/sec), which is consistent with the observation that *cis*-TmeA achieves
187 peak actin intensity roughly 20 seconds later than wild-type or *cis*-TarP strains (Fig. 1B). Deletion of either
188 TmeA or TarP attenuated actin recruitment kinetics by 2-fold and 5-fold, respectively, relative to wild-type
189 *Chlamydia* (ΔTmeA=0.178 fold/sec, ΔTarP=0.054 fold/sec). Actin kinetics were further restricted by
190 simultaneous deletion of both TmeA and TarP (ΔTmeA/ΔTarP=0.031 fold/sec), yielding a nearly 10-fold
191 reduction in the rate of actin recruitment. Altogether, these data suggest that optimal rapid actin
192 recruitment is an effector-driven process that relies on both TarP and TmeA. Furthermore, we observed
193 that actin kinetics were more severely attenuated in strains that lack TarP (ΔTarP, ΔTmeA/ΔTarP),
194 suggesting that TarP is the major determinant of actin recruitment kinetics, and that TmeA has a minor
195 role in rapid actin recruitment.

196 Despite exhibiting variability in recruitment kinetics, we noted that the actin turnover rate for
197 wild-type, *cis*-TmeA, and *cis*-TarP were all comparably fast (Wild-type=0.082 fold/sec, *cis*-TmeA=0.104
198 fold/sec, *cis*-TarP=0.117 fold/sec) (Fig. 1E). Interestingly, we observed that deletion of either TmeA or TarP
199 roughly halved the turnover rate of actin (ΔTmeA=0.068 fold/sec, ΔTarP=0.043 fold/sec) compared to
200 wild-type, suggesting that TmeA and TarP influence both actin recruitment and turnover. Notably, TmeA

201 deletion exerted a greater impact on the kinetics of actin turnover than recruitment, whereas TarP
202 deletion greatly impacted both actin recruitment and turnover. Furthermore, the duration of actin
203 turnover was substantially reduced in strains that lack TarP, lasting on average for 120 seconds before
204 actin intensity returned to near-background levels (Fig. S4). In contrast, turnover lasted for an average of
205 380 seconds in wild-type and *cis*-complemented strains, and 240 seconds for the ΔTmeA strain.
206 Collectively, these data support a model wherein TarP and TmeA determine the quality of actin dynamics.
207 Thus far, we have identified four relevant attributes of actin dynamics that exhibit variability at
208 the population level upon deletion of TarP and/or TmeA: i) recruitment rate, ii) recruitment intensity iii)
209 turnover rate, and iv) turnover duration. To clarify how recruitment and turnover are regulated at the
210 single EB level, we calculated all four attributes for each individual recruitment event represented in the
211 population-level data. Using these values, we conducted a series of pairwise correlation analyses to
212 identify the relationship between attributes (Table 1). Surprisingly, despite the link between rapid actin
213 recruitment and rapid turnover present at the population level, we noted that individual EBs exhibited
214 moderate-to-weak correlation between the rate of recruitment and turnover, implying a level of
215 independence between the two phases. This could be due to the presence of predetermining factors that
216 variably influence the recruitment and turnover rates of actin at each invasion event. Some examples
217 include the local concentration of invasion-relevant translocated effectors, the density of pre-formed
218 actin networks which serve as sites for initial or additional actin polymerization, or the abundance of
219 signaling co-receptors. These local variations could result in variable actin dynamics at the individual level
220 that become less apparent when analyzed at the population level.
221
222 **Table 1: Pairwise correlation analyses of actin kinetics following deletion or *cis*-complementation of**
223 **TarP and TmeA**

	Recruitment Rate vs. Turnover Rate	Recruitment Rate vs. Intensity	Turnover Rate vs. Intensity	Turnover Duration vs. Intensity
Actin *cis* -TmeA	r= 0.108	r= 0.168	r= 0.446	r= 0.175
Actin ΔTmeA	r= 0.246	r= 0.277	r= 0.47	r= 0.068
Actin *cis* -TarP	r= 0.338	r= 0.568	r= 0.49	r= 0.183
Actin ΔTarP	r= 0.535	r= 0.177	r= 0.654	r= 0.364
ΔTmeA/ΔTarP	r= 0.283	r= 0.673	r= 0.565	r= 0.21

Negligible	Weak	Moderate	Strong	Very Strong
0.00 - 0.19	0.20 - 0.39	0.40 - 0.59	0.60 - 0.79	0.8+

We also observed a consistently strong correlation between the rate of actin turnover and its corresponding peak intensity, which was not observed during the recruitment phase. This implies that the rate of turnover is dictated by the amount of polymerized actin, or the density of the actin network formed at the peak of recruitment. As a result, the duration of actin turnover is reasonably consistent among individual EBs despite exhibiting substantial variation in actin intensity, as indicated by weak correlation between turnover duration and actin intensity. Finally, we noted that ΔTarP EBs, and to a lesser extent ΔTmeA/ΔTarP EBs, appear to be regulated distinctly from strains that possess TarP. In particular, ΔTarP exhibited a strong correlation between recruitment and turnover rates and moderate correlation between turnover duration and intensity (Table 1). Coupled with the poor actin retention and impaired actin kinetics observed at the population level, these observations imply that TarP plays a key role in coordinating actin kinetics at both the individual and population level. Together, these data emphasize the importance of the secreted effectors TarP and TmeA in generating a stable actin network with rapid recruitment and turnover kinetics. Additionally, our findings impress the importance of quantitatively analyzing individual invasion events to identify relevant characteristics that are masked in population-level analyses.

Arp2/3 recruitment dynamics at entry sites displays dependence on TmeA and TarP

243 One explanation for impaired actin kinetics following TarP and TmeA deletion is that loss of either effector
244 prevents optimal recruitment of the actin nucleator Arp2/3. Indeed, a recent study suggested that the
245 respective signal transduction capabilities of TarP and TmeA form a functional collaboration that enhances
246 recruitment of Arp2/3 and increases the rate of actin polymerization [23,24]. As such, we monitored the
247 recruitment of fluorescent Arp3 at the entry sites of wild-type, *cis*-complemented, or effector deletion
248 strains in order to assess the contribution of effector collaboration on Arp2/3 recruitment during invasion
249 (Fig. 2). We observed recruitment of Arp3 in all strains except for ΔTmeA/ΔTarP, indicating that Arp2/3
250 recruitment is contingent upon the presence of either TarP or TmeA (Fig. 2A,B). We noted that *cis*-TmeA
251 EBs required an additional 20 seconds to recruit Arp3 at a comparable intensity to either wild-type or *cis*-
252 TarP strains (Fig. 2B), which is consistent with the slight delay in peak actin intensity observed prior (Fig.
253 1B). Surprisingly, TmeA deletion did not substantially alter the intensity of Arp3 recruitment, whereas TarP
254 deletion resulted in dim and transient Arp3 recruitment (Fig. 2B). In conjunction with the absence of Arp3
255 recruitment in the ΔTmeA/ΔTarP strain, these data suggest that both TarP and TmeA are independently
256 capable of Arp3 recruitment. Nevertheless, the apparent differences between the Arp3 recruitment
257 profiles of ΔTarP and ΔTmeA are inconsistent with a synergetic interaction between the effectors, instead
258 indicating that Arp2/3 recruitment is primarily driven by TarP. However, we observed that Arp3
259 recruitment at the entry sites of ΔTmeA EBs was visibly more transient than Arp3 recruitment in either
260 *cis*-TmeA or wild-type strains, indicating a potential role for TmeA in promoting stable recruitment of
261 Arp2/3.

262 In order to clarify the respective contributions of TarP and TmeA toward Arp2/3 recruitment, we
263 monitored the kinetics of Arp3 recruitment and turnover for each strain tested above. We noted that the
264 recruitment kinetics of Arp3 were largely similar in all strains except for ΔTarP, which recruited Arp3 nearly
265 4-fold slower than wild-type or *cis*-complemented strains (Wild-type=0.079 fold/sec, ΔTarP=0.020
266 fold/sec) (Fig. 2C, Table S2). Consistent with the delay in peak Arp3 intensity, *cis*-TmeA EBs possessed a

267 slightly lower median Arp3 recruitment rate (*cis*-TmeA=0.059 fold/sec) than wild-type or *cis*-TarP EBs,
268 although the distribution of rates is comparable among all three strains. Finally, TmeA deletion did not
269 alter the recruitment kinetics of Arp3, as ΔTmeA EBs recruited Arp3 at a rate comparable to wild-type or
270 *cis*-TarP EBs (ΔTmeA= 0.091 fold/sec, *cis*-TarP= 0.095 fold/sec). Altogether, these data indicate that while
271 TmeA is independently capable of recruiting Arp2/3, it does so at a far slower rate than strains which
272 contain TarP. As such, we conclude that the presence of TarP is a key determinant of rapid Arp3
273 recruitment.

274 During imaging, we noted that Arp3 recruitment by ΔTmeA EBs was visibly more transient than
275 cis-TmeA or wild-type EBs, which may indicate that TmeA signaling is necessary for optimal retention of
276 Arp2/3. In agreement with this, we found that the turnover rate of Arp3 was substantially higher at ΔTmeA
277 entry sites (ΔTmeA=0.091 fold/sec) than wild-type (0.035 fold/sec) or cis-TmeA (0.054 fold/sec) (Fig. 2D).
278 Furthermore, pairwise correlation analyses revealed that the Arp3 turnover rate of ΔTmeA EBs was
279 positively correlated with both its corresponding recruitment rate and its recruitment intensity, together
280 implying that rapid and intense Arp3 recruitment results in proportionally rapid Arp3 turnover (Table 2).
281 Collectively, this demonstrates that TmeA signaling contributes to the stability of Arp2/3 following its
282 recruitment, such that TmeA deletion results in poor retention of Arp2/3, attenuated actin kinetics, and
283 inefficient engulfment of *Chlamydia*. Meanwhile, TarP deletion resulted in a drastic attenuation of Arp3
284 turnover kinetics relative to wild-type or *cis*-TarP strains (*cis*-TarP=0.070 fold/sec, ΔTarP=0.023 fold/sec),
285 indicating that loss of TarP signaling dramatically alters both recruitment and turnover of Arp2/3. In
286 summary, these data indicate that TarP and TmeA signaling are mutually important for optimal Arp2/3
287 kinetics, each regulating distinct attributes of Arp2/3 recruitment. TarP signaling is associated with robust
288 Arp2/3 recruitment, while TmeA signaling is required to maintain Arp2/3 stability within entry sites.
289 Coupled with the attenuated actin kinetics and poor invasion efficiency of ΔTarP and ΔTmeA strains (Fig.

290 1), we conclude that efficient invasion is reliant upon the co-regulation of Arp2/3 kinetics by TarP and
291 TmeA.
292
293 **Table 2: Pairwise correlation analyses of Arp3 kinetics following deletion or *cis*-complementation of**
294 **TarP and TmeA**

	Recruitment Rate vs. Turnover Rate	Recruitment Rate vs. Intensity	Turnover Rate vs. Intensity	Turnover Rate vs. Duration
Arp3 *cis* -TmeA	r= 0.004	r= 0.657	r= 0.294	r= 0.224
Arp3 ΔTmeA	r= 0.549	r= 0.377	r= 0.775	r= 0.447
Arp3 *cis* -TarP	r= 0.003	r= 0.319	r= 0.304	r= 0.269
Arp3 ΔTarP	r= 0.612	r= 0.519	r= 0.452	r= 0.259

Negligible	Weak	Moderate	Strong	Very Strong
0.00 - 0.19	0.20 - 0.39	0.40 - 0.59	0.60 - 0.79	0.8+

295
296
297 **Formin 1 is recruited during invasion in a TarP-dependent and TmeA-independent manner**
298 Despite the mutual importance of TarP and TmeA toward efficient invasion, we noted that the recruitment
299 profiles of both actin and Arp3 differed substantially between ΔTarP and ΔTmeA strains. In particular, we
300 noted that the kinetics of actin and Arp3 were more substantially attenuated during ΔTarP invasion than
301 ΔTmeA invasion. One possible explanation for this difference may be the presence of additional TarP-
302 specific factors which influence the kinetics of Arp2/3 and actin. Arp2/3 is known to collaborate with a
303 class of actin nucleators known as formins, which generate elongated actin filaments by substantially
304 increasing the polymerization rate of actin. These elongated filaments are bound by Arp2/3, generating
305 branched actin filaments that may be acted upon by formins, consequently increasing the kinetics of both
306 Arp2/3 and actin recruitment. As such, we tested whether formins are recruited during invasion, and
307 whether their recruitment was contingent upon the presence of TarP or TmeA. We observed the robust
308 recruitment of Formin 1 (Fmn1) at the entry sites of wild-type, *cis*-complemented, and ΔTmeA strains,
309 which was absent in ΔTarP and ΔTmeA /ΔTarP strains, suggesting that Fmn1 recruitment is TarP-

310 dependent (Fig. 3A,B). TmeA deletion did not appreciably alter the recruitment intensity of Fmn1 relative
311 to either *cis*-TmeA or wild-type *Chlamydia* (wild-type=10.7 ± 1.7 fold, *cis*-TmeA=9.9 ± 1.4 fold, ΔTmeA=8.5
312 ± 0.6 fold), indicating that recruitment of Fmn1 is mediated primarily by TarP and largely independent of
313 TmeA. Additionally, we observed that Fmn1 recruitment was often persistent among wild-type and cis-
314 complemented strains, resulting in a protracted turnover phase wherein Fmn1 is retained for 300+
315 seconds after peak intensity (Fig. 3B). This phenomenon was absent during ΔTmeA invasion; rather, Fmn1
316 recruitment in this strain rapidly achieved peak intensity before equally rapidly returning to basal
317 intensity. Finally, ΔTarP and ΔTmeA /ΔTarP EBs failed to recruit Fmn1, yielding only trace RFP signals at
318 sites where these strains contact host cells. Collectively, these data indicate that Fmn1 is recruited during
319 invasion in a TarP-dependent manner, while TmeA signaling appears to influence the retention of Fmn1
320 at invasion sites, akin to its proposed role in supporting Arp2/3 stability.

321 To further examine the influence of TarP and TmeA signaling on Fmn1 recruitment, we compared
322 the kinetics of Fmn1 recruitment between strains (Fig. 3C, Table S3). Once again, we observed that cis-
323 TmeA EBs exhibited a marginally slower Fmn1 recruitment rate (cis-TmeA=0.077 fold/sec) than either
324 wild-type (0.106 fold/sec) or cis-TarP (0.127 fold/sec) EBs, which mirror our findings regarding the kinetics
325 of actin and Arp3. Thus, although *cis*-TmeA recruitment kinetics are generally slightly reduced relative to
326 wild-type *Chlamydia*, the pattern of deviation is consistent between actin, Arp3, and Fmn1, indicating that
327 the recruitment of these proteins is co-regulated. Fmn1 recruitment kinetics were not altered by TmeA
328 deletion (ΔTmeA=0.092 fold/sec) but were reduced by over 10-fold following TarP deletion (ΔTarP=0.013
329 fold/sec). Together, this implies that TarP is the primary determinant of Fmn1 and Arp2/3 recruitment
330 kinetics.

331 Interestingly, we noted that ΔTmeA EBs achieved a significantly higher Fmn1 turnover rate than
332 wild-type *Chlamydia* (Wild-type=0.041 fold/sec, ΔTmeA=0.070 fold/sec), which is reminiscent of the
333 pattern observed during Arp3 turnover (Fig. 3D). Indeed, correlation analyses indicated that, similar to

334 Arp3, the turnover rate of Fmn1 among ΔTmeA EBs was correlated with its corresponding recruitment
335 rate and recruitment intensity (Table 3), suggesting that Fmn1 evacuates ΔTmeA entry sites at a rate
336 proportional to its recruitment. Thus, although TmeA signaling has a negligible impact on the recruitment
337 kinetics of Fmn1 and Arp2/3, it is essential for stable association of these actin nucleators within
338 *Chlamydia* entry sites. In contrast, TarP deletion prevented the recruitment of Fmn1, resulting in a nearly
339 negligible Fmn1 turnover rate (ΔTarP=0.009 fold/sec). Collectively, these data reveal that the actin
340 nucleators Arp2/3 and Fmn1 are robustly recruited during invasion to establish an intense and highly
341 localized actin network with rapid kinetics. TarP secretion is essential for Fmn1 recruitment, and is
342 required for optimal Arp2/3 recruitment, indicating that TarP is a key regulator of actin nucleator
343 recruitment. In contrast, TmeA signaling was revealed to promote stable retention of actin nucleators
344 within *Chlamydia* entry sites, which was crucial for efficient pathogen engulfment. Thus, despite having
345 only a limited effect on the recruitment kinetics of actin and its nucleators, TmeA signaling may be
346 necessary for optimal activation, and thus retention of Arp2/3. A failure to activate and integrate Arp2/3
347 within actin networks would limit the number of binding sites for Fmn1, effectively promoting its turnover
348 and restricting the influence of Fmn1 and Arp2/3 on actin remodeling.
349
350 **Table 3: Pairwise correlation analyses of Fmn1 kinetics following deletion or *cis*-complementation of**
351 **TarP and TmeA**

	Recruitment Rate vs. Turnover Rate	**Recruitment Rate vs. Intensity**	**Turnover Rate vs. Intensity**	**Turnover Rate vs. Duration**
Fmn1 *cis* -TmeA	r= 0.516	r= 0.654	r= 0.250	r= 0.088
Fmn1 ΔTmeA	r= 0.647	r= 0.196	r= 0.313	r= 0.498
Fmn1 *cis* -TarP	r= 0.333	r= -0.02	r= 0.28	r= 0.208
Fmn1 ΔTarP	r= 0.935	r= 0.658	r= 0.7	r= 0.592

Negligible	Weak	Moderate	Strong	Very Strong
0.00 - 0.19	0.20 - 0.39	0.40 - 0.59	0.60 - 0.79	0.8+

352
353

354 **Inhibition of filamentous and branched nucleation of actin at the sites of entry reduces invasion**
355 **efficiency and significantly alters actin recruitment kinetics**

356 As a consequence of actin remodeling, *Chlamydia* reconfigures host membranes into invasion-associated
357 structures such as hypertrophic microvilli, which assist in the capture and engulfment of invading bacteria.
358 These structures are associated with the actin elongating properties of formins such as Fmn1, which is
359 recruited during invasion in a TarP-dependent manner (Fig. 3). This finding confirms an earlier observation
360 from a previously published RNA interference screen in Drosophila S2 cells that identified formin and
361 Diaphanous as being required for *Chlamydia* infection. In light of these observations, we transfected Cos7
362 cells with GFP-fusion constructs of the mammalian Diaphanous homologs mDia1 (mEmerald-mDia1) and
363 mDia2 (mEmerald-mDia2) and tracked their recruitment around invading *Chlamydiae* (Fig. 4A). We
364 identified recruitment of Fmn1, mDia1, and mDia2 at wild-type *Chlamydia* entry sites, indicating that
365 multiple species of formin are recruited during invasion. We utilized the pan-formin inhibitor SMIFH2 to
366 pharmacologically inhibit formin activity in order to circumvent the observed cytotoxicity associated with
367 simultaneous knockdown of Fmn1, mDia1, and mDia2. SMIFH2 is ideally suited for this purpose, since it
368 inhibits all three formin species by blockade of their conserved formin-homology 2 (FH2) domains, thus
369 preventing formin-mediated actin polymerization [43]. Importantly, we utilized SMIFH2 at a relatively low
370 concentration (10µM), which is approximately 4-fold lower than the effective concentration to inhibit
371 myosin superfamily proteins (Fig. S5) [44]. Additionally, we employed the Arp2/3 inhibitor CK666, which
372 prevents Arp2/3 branching activity by occluding the actin binding cleft between subunits Arp2 and Arp3
373 [45]. The Arp2/3 complex is known to be required for efficient invasion [9], and thus serves as a basis for
374 comparison regarding the potential effects of formin inhibition .

375 First, we investigated whether the activities of formin and Arp2/3 are necessary for invasion by
376 comparing the efficiency of *Chlamydia* invasion in the presence and absence of SMIFH2, CK666, or both
377 (Fig. 4B). Cos7 cells were pre-treated with inhibitors for 60 min prior to inoculation with *C. trachomatis*

378 serovar L2 EBs. We normalized our data to the efficiency of invasion in absence of inhibitor in order to
379 directly compare the effects of formin and/or Arp2/3 inhibition on invasion. Inhibiting the activity of either
380 formin or Arp2/3 yielded a comparable impediment to invasion, each reducing invasion efficiency by
381 roughly 40%, while simultaneous inhibition of formin and Arp2/3 reduced invasion efficiency by 60%.
382 Together, these data suggest that while formin and Arp2/3 activity are independently important for
383 invasion, their combined inactivation causes a more substantial impediment to pathogen entry.

384 To determine if this impairment in *Chlamydia* internalization is due to a deficiency in actin
385 polymerization, we quantified the recruitment of GFP-actin at the site of invasion in the presence or
386 absence of these inhibitors by time-lapse imaging of live Cos7 cells (Fig. 4C). *Chlamydia* robustly recruited
387 actin in absence of inhibitor at an intensity of nearly 20-fold above background, which was reduced by
388 over 10-fold following application of SMIFH2 or CK666. Interestingly, dual inhibition of formin and Arp2/3
389 did not further reduce actin recruitment but yielded a form of actin recruitment that was substantially
390 slower and much more persistent, often failing to turn over throughout the duration of the experiment
391 (Video S2). Altogether, these data indicate that the activities of formin and Arp2/3 are manipulated by
392 *Chlamydia* to enhance actin remodeling, and that inhibition of either nucleator yields a deficiency in
393 pathogen entry.

394

395 **Recruitment and turnover of actin are slowed by inhibition of filamentous and branched actin**
396 **nucleators**

397 Earlier, we noted that mutant *Chlamydia* strains which failed to recruit and retain Fmn1 and/or Arp2/3
398 suffered defects to both actin kinetics and invasion efficiency, suggesting that stable association of both
399 nucleators is necessary for optimal actin kinetics. Our data indicate that inhibition of either Arp2/3 or
400 formin induces a comparable defect to both actin recruitment intensity and invasion efficiency, intimating
401 that their respective actin branching and elongating properties are equally important for robust actin

402 kinetics. To test this claim, we compared the kinetics of actin recruitment and turnover at the invasion
403 sites of cells treated with inhibitors for Arp2/3 and/or formin (Fig. 4D,E, Fig. S6). Inhibitor treatment
404 reduced the rate of recruitment by 3-4 fold compared to mock-treatment (Mock=0.285 fold/sec,
405 SMIFH2=0.082 fold/sec, CK666=0.072 fold/sec) (Fig. 4D) and altered the recruitment profile across
406 multiple parameters, ultimately resulting in a narrower range of recruitment rates (Table S4). Together,
407 this indicates that when only one nucleator is operational, the rate of actin recruitment is slower and
408 more consistent. Furthermore, co-inhibition of formin and actin yielded an even more narrow range of
409 actin recruitment rates (Range CK+SMI=0.044) and reduced the overall rate by 10-fold (CK+SMI=0.015
410 fold/sec). Since actin recruitment was not completely ablated by dual-inhibition of formin and Arp2/3,
411 these data imply the presence of a formin- and Arp2/3-independent mechanism of actin recruitment at
412 the site of invasion. However, the resultant actin network polymerizes very slowly and more uniformly
413 than the actin network created by host actin nucleators. Collectively, this suggests that formin and Arp2/3
414 activity contributes to efficient invasion by enhancing the recruitment kinetics of actin, resulting in the
415 rapid establishment of a robust actin network at the site of invasion.

416 Interestingly, the turnover phase of actin kinetics shares many features in common with the
417 recruitment phase (Fig. 4E). Inhibition of formin or Arp2/3 reduced the median turnover rate by 3-4 fold
418 compared to mock treatment (Mock=0.096 fold/sec, SMIFH2=0.026 fold/sec, CK666=0.031 fold/sec) (Fig.
419 4E, Table S4), which is comparable to the reduction observed in the recruitment phase of actin. Moreover,
420 inhibition of formin or Arp2/3 also altered the turnover profile of actin, generating a narrower range of
421 turnover rates (Table S4). Given that recruitment and turnover are comparably altered by inhibition of
422 formin or Arp2/3, our data imply a link between these phases such that rapid/slowed recruitment is paired
423 with rapid/slowed turnover. This is also true for when formin and Arp2/3 are simultaneously inhibited,
424 which reduces the turnover rate of actin by over 10-fold (CK+SMI=0.005 fold/sec) compared to mock
425 treatment. To confirm that comparisons derived from the violin plots are reflective of the overall kinetics

426 for each recruitment condition, we performed a linear regression analysis on the mean rate of recruitment
427 and turnover for each phase (Fig. S6). We noted that the trends observed in violin plots (Fig. 4D,E) were
428 also observed in the averaged rate slopes for all conditions tested (Fig. S6A,B), indicating that differences
429 between individual rate distributions are reflective of the overall kinetics for each condition. In sum, our
430 data indicate that inhibition of host actin nucleators substantially impairs rapid actin recruitment and
431 turnover at the site of invasion, while only having a minor effect on the slow, lingering phase of actin
432 turnover.

433 Finally, we wanted to evaluate whether the trends observed in actin recruitment and turnover at
434 the population level were preserved at the single EB level (Table 4). Consistent with the correlation
435 analyses conducted on *cis*-TarP and *cis*-TmeA, we observed that mock-treated wild-type *Chlamydia*
436 exhibited negligible correlation between the rate of actin recruitment and turnover. In contrast, inhibition
437 of either formin or Arp2/3 altered this relationship such that a moderate correlation existed between
438 recruitment and turnover rates. Interestingly, we observed that the rate of actin recruitment and turnover
439 exhibited a moderate correlation following inhibition of Arp2/3, and negligible correlation upon inhibition
440 of formin. Collectively, these data suggest that formin and Arp2/3 uniquely contribute to actin dynamics
441 at entry sites, such that inhibition of either nucleator produces divergent effects on the regulation of actin
442 networks among individual EBs. Notwithstanding, we conclude that optimal kinetics of actin recruitment
443 are achieved when both formin and Arp2/3 are active, suggesting that *Chlamydia* relies on the nucleation
444 of both branched and filamentous actin for optimal actin remodeling.

445

446 **Table 4: Pairwise correlation analyses of actin kinetics following inhibition of formin and Arp2/3**

	Recruitment Rate vs. Turnover Rate	Recruitment Rate vs. Intensity	Turnover Rate vs. Intensity	Turnover Duration vs. Intensity
Actin Untreated	r= 0.173	r= 0.371	r= 0.269	r= 0.043
Actin SMIFH2	r= 0.581	r= 0.084	r= -0.084	r= 0.382
Actin CK666	r= 0.428	r= 0.477	r= 0.472	r= 0.196
Actin CK+SMI	r= -0.003	r= -0.059	r= 0.334	r= 0.098

Negligible	Weak	Moderate	Strong	Very Strong
0.00 - 0.19	0.20 - 0.39	0.40 - 0.59	0.60 - 0.79	0.8+

Formin and Arp2/3 are co-recruited to the site of invasion

The observation that formin and Arp2/3 promote actin recruitment during invasion raise the possibility that these nucleators act collaboratively, thereby enhancing the capacity of *Chlamydia* to generate actin-rich invasion structures. If nucleator collaboration does indeed play a role in invasion, we expect that both formin and Arp2/3 will be present within a single invasion event, and that inhibiting either nucleator will impair recruitment of its collaboration partner. Although multiple species of formin were recruited during invasion (Fig. 4A), we chose to monitor Fmn1 since this protein was specifically identified in a prior siRNA screen of cytoskeletal effectors with a role in *Chlamydia* invasion [46]. We observed that GFP-Fmn1 was robustly recruited during invasion and experienced a substantial defect in recruitment upon pharmacological inhibition of Arp2/3 (Fig. 5A). Likewise, GFP-Arp3, which has been validated as a marker for the Arp2/3 complex [47], was robustly recruited during invasion and also demonstrated reduced recruitment following inhibition of formin (Fig. 5B). Altogether, this indicates that recruitment of Fmn1 and Arp2/3 are reciprocally enhanced by their respective actin nucleating functions and subsequent actin polymerization.

Next, we determined whether Fmn1 and Arp2/3 are co-recruited within individual invasion events, thus providing the necessary context for nucleator collaboration. To do this, we co-expressed GFP-Fmn1 and mCherry-Arp3 and measured the recruitment of both proteins during invasion by time-lapse imaging followed by fluorescence quantification (Fig. 5C). We observed that all events we monitored

467 exhibited both Fmn1 and Arp3 accumulation, indicating that they are co-recruited by *Chlamydia*. To
468 measure the timing of their arrival, we normalized the intensity of recruitment to the maximal MFI of each
469 protein at each timepoint, expecting that any delays in protein recruitment would be represented by a
470 shift in their recruitment profile. In contrast, we noted that the recruitment profiles of both Fmn1 and
471 Arp3 were remarkably similar and achieved maximal MFI at the same timepoint, indicating that both
472 proteins arrived at the entry site within 20 seconds of each other, the temporal resolution of our imaging
473 protocol. Given both the simultaneous recruitment of Fmn1 and Arp2/3 and the reciprocal dependence
474 of their respective activities for optimal recruitment, we conclude that Fmn1 and Arp2/3 collaborate
475 during invasion to promote actin recruitment. This observation is particularly novel, given that there are
476 no other instances of the utilization of Fmn1 by bacterial pathogens. Lastly, given the robust recruitment
477 of Fmn1, we were interested in whether other formin species such as DRFs, which require upstream
478 activation by Rho-GTPases, could also participate in nucleator collaboration. To this end, we found that
479 mEmerald-mDia1 and mEmerald-mDia2 were also recruited during invasion, and that their recruitment
480 was impaired by Arp2/3 inhibition (Fig. 5D), suggesting that both DRF and non-DRF formins collaborate
481 with Arp2/3 during invasion.
482
483 **Recruitment and turnover profiles of Fmn1 and Arp2/3 are altered by reciprocal inhibition of their**
484 **respective actin nucleation function**
485 Using the same methodology to evaluate actin kinetics (Fig. 1D,E), we compared the recruitment and
486 turnover profiles of Fmn1 and Arp2/3 to more closely evaluate how inhibition of each protein alters their
487 recruitment and turnover dynamics during invasion. Compared to mock treatment, inhibition of Fmn1
488 decreased the rate of Arp3 recruitment by 34 percent (Mock=0.079 fold/sec, SMIFH2=0.052 fold/sec),
489 while inhibition of Arp2/3 reduced the rate of Fmn1 recruitment by 47 percent (Mock=0.106 fold/sec,
490 CK666=0.056 fold/sec) (Fig. 5E, Table S5). Together, this indicates that collaboration between the activities

491 of Fmn1 and Arp3 not only enhance the rate of actin recruitment (Fig. 4D), but also reciprocally enhance
492 their respective recruitment rates. As such, we conclude that Arp2/3-mediated actin branching produces
493 additional barbed-ends for Fmn1 binding; reciprocally, Fmn1 activity produces elongated actin filaments
494 which allow efficient incorporation of Arp2/3 into actin networks generated by invading *Chlamydiae*.
495 Shifting our focus onto turnover, we found that CK666 treatment reduced the turnover rate of Fmn1 by
496 4-fold compared to mock-treatment (Mock=0.041 fold/sec vs. CK666=0.009 fold/sec), while SMIFH2
497 treatment did not significantly alter the rate of Arp3 turnover (Mock=0.019 fold/sec vs. SMIFH2=0.024
498 fold/sec) (Fig. 5F, Table S5). Furthermore, we found that the turnover rate of Fmn1 among individual EBs
499 was moderately correlated with its corresponding peak intensity (r=0.402), which was not observed upon
500 inhibition of Arp2/3 (r=0.074) (Table 5). This discrepancy may be due to a relative lack of Fmn1 binding
501 sites coupled with poor actin turnover following inhibition of Arp2/3 (Fig. 4E), such that the turnover rate
502 of Fmn1 is dictated by binding site availability in inhibitor-treated cells. In contrast, rapid turnover of Fmn1
503 in mock-treated cells is potentially due to the relative abundance of Fmn1 binding sites coupled with rapid
504 actin turnover, such that Fmn1 turnover is likely dictated by actin turnover dynamics. Meanwhile, we
505 noted that SMIFH2 treatment did not alter the turnover rate of Arp2/3 (Fig. 5F), nor did it exert any
506 observable effect on the regulation of Arp2/3 turnover as indicated by pairwise correlation analysis (Table
507 5). Thus, we conclude that turnover of Fmn1 and Arp2/3 are governed by different mechanisms, wherein
508 Arp2/3 turnover occurs via a process that is independent of Fmn1 activity.
509
510 **Table 5: Pairwise correlation analyses of Fmn1 and Arp3 kinetics in presence and absence of inhibitor.**

	Recruitment Rate vs. Turnover Rate	Recruitment Rate vs. Intensity	Turnover Rate vs. Intensity	Turnover Duration vs. Intensity
Fmn1 Untreated	r= 0.367	r= 0.443	r= 0.398	r= 0.087
Fmn1 CK666	r= 0.119	r= 0.248	r= 0.074	r= 0.268
Arp3 Untreated	r= 0.395	r= 0.788	r= 0.596	r= 0.367
Arp3 SMIFH2	r= 0.487	r= 0.567	r= 0.582	r= 0.101

Negligible	Weak	Moderate	Strong	Very Strong
0.00 - 0.19	0.20 - 0.39	0.40 - 0.59	0.60 - 0.79	0.8+

Overall, this study highlights the remarkable complexity of the interaction between invading *Chlamydia* and the host cytoskeleton, identifying several novel interactions which culminate to support rapid actin kinetics and efficient pathogen engulfment. In play are at least two effectors (TarP and TmeA), signaling from accessory cell surface receptors, and the existing cross-regulatory machinery of actin nucleation, polymerization, and turnover (Fig. 6). Adding to this complexity is the various functional interactions between multiple formins/formin-like proteins with Arp2/3. The recruitment and turnover kinetics of mDia1 and mDia2 were similarly sensitive to CK666-mediated inhibition of the Arp2/3 complex (Fig. S7, Table S6,7), suggesting that multiple formin species may participate in nucleator collaboration. Thus, our data indicate that filamentous and branched actin nucleation and polymerization constitute a fundamental interaction in which formins in general collaborate with Arp2/3 during invasion following their recruitment by TarP and TmeA.

525

526 **Discussion:**

527 In this study, we demonstrated that co-regulation of Arp2/3 kinetics by the *Chlamydia* effectors TarP and
528 TmeA, coupled with TarP-dependent recruitment of Fmn1, led to the establishment of a robust actin
529 modulatory network at pathogen entry sites to promote internalization. By monitoring the kinetics of
530 recruitment, we identified a functional collaboration between the actin nucleating and polymerizing
531 activities of formin and Arp2/3, which accelerated the rate of actin recruitment as well as reciprocally
532 enhancing the recruitment of actin nucleators. Furthermore, we emphasized the necessity for actin
533 turnover in order to achieve pathogen internalization and demonstrated that signaling from both TarP
534 and TmeA were essential for rapid actin turnover and optimal pathogen internalization.

535

536 *Actin dynamics at the site of chlamydial invasion*

537 Intracellular pathogens often target the actin cytoskeleton during entry, leading to robust actin
538 recruitment and subsequent formation of invasion-associated structures. Although *Chlamydia* has been
539 demonstrated to use a plurality of entry mechanisms to achieve internalization (filopodial capture,
540 clathrin-mediated endocytosis, macropinocytosis, membrane ruffling), we were unable to distinguish the
541 actin dynamics associated with each mechanism. Therefore, while our study impressed the importance of
542 TarP and TmeA signaling toward optimal actin kinetics, we were unable to identify whether deletion of
543 either effector altered which entry mechanisms were utilized by invading *Chlamydiae*. Likewise, further
544 study is required to determine the role of formin and Arp2/3 toward the assembly of each invasion-
545 associated structure, and whether inhibition of either actin nucleator prevents the utilization of a given
546 entry mechanism.

547 Relative to *Chlamydia*, actin recruitment in other intracellular bacteria is longer lived [17,48],
548 lasting on the order of 5-15 minutes; in contrast, we have shown that *Chlamydia* actin recruitment is both

549 robust and transient, emphasizing the importance of rapid actin accumulation and turnover during its
550 invasion. To our knowledge, no equivalent study on the rate of actin recruitment during the internalization
551 of an intracellular pathogen has been conducted, thus a direct comparison on the kinetics of actin
552 recruitment between pathogens is not possible. As such, we believe our study provides a valuable new
553 approach that could be used in future studies to improve contextualization of protein dynamics for other
554 intracellular pathogens in addition to *Chlamydia*.

555 Using these tools, we found that secretion of the *Chlamydia* effectors TarP and TmeA led to rapid
556 recruitment of actin, which was due in part to the collaboration between Fmn1 and Arp2/3. One
557 explanation for the high rate of recruitment observed in our study is the establishment of a positive
558 feedback loop, where actin branching by Arp2/3 and filament elongation by Fmn1 create additional nodes
559 for Arp2/3 and Fmn1 to bind (Fig. 6). Iterations of this process would account for both the high recruitment
560 rate of actin in addition to providing an explanation for why inhibition of Fmn1 and Arp2/3 comparably
561 affect the recruitment rate of actin. However, this model does not immediately make apparent why actin
562 recruitment is transient, nor does it provide explanation for the slow and persistent actin recruitment
563 observed following inhibition of both formin and Arp2/3. Other host actin nucleators such as SPIRE, APC,
564 or Cordon-bleu have not yet been identified in siRNA screens of invasion-associated proteins, nor has any
565 evidence of their involvement in *Chlamydia* invasion been given [49]. Although TarP has been shown via
566 pyrene assay to serve as an actin nucleator, it remains unknown whether it also performs this function in
567 cell lines or *in-vivo* [50]. However, based on results described here, TarP deletion drastically impaired the
568 kinetics of recruitment and turnover of both actin and its nucleators, indicating that actin nucleation is
569 predominantly driven by host nucleators rather than TarP itself.

570 In addition to rapid actin recruitment, we also observed a two-phase actin turnover process
571 starting with a brief fast turnover phase (100-180 sec) followed by a prolonged slow turnover phase (400-
572 600 sec). The rate of actin turnover was reduced by deletion of either TmeA or TarP, or by inhibition of

573 either formin or Arp2/3, collectively indicating that rapid actin turnover is an effector-driven process
574 which is contingent upon the activity of actin nucleators. Although this process is relatively understudied
575 in intracellular bacterial invasion, actin turnover is of clear importance for bacterial internalization, as
576 dysregulation of actin turnover machinery commonly impairs bacterial entry. For instance, impairment or
577 hyperactivation of the actin depolymerizing protein ADF-cofilin restricts internalization of *S. enterica*,
578 while overexpression of the ADF-cofilin kinase LIMK reduced *L. monocytogenes* ruffle formation and
579 internalization [51,52]. In *C. burnetii* and *L. monocytogenes*, time-course experiments tracking actin
580 recruitment also demonstrated a clear spike in actin recruitment followed by a two-phase rapid/residual
581 turnover profile [48,52]. Thus, the actin turnover profile observed in our study may simply reflect normal
582 actin turnover dynamics, as opposed to being intrinsic to invading *Chlamydia*. Given the importance of
583 host actin depolymerization factors like gelsolin, ADF-cofilin and their regulators for efficient
584 internalization of other intracellular bacteria, it may be that such proteins are also responsible for actin
585 turnover during *Chlamydia* invasion [40,53–55]. Indeed, an siRNA screen of *C. muridarum* invasion-
586 associated proteins identified four actin depolymerization factors, ADF-cofilin, cyclase associated protein
587 (CAP), Coronin, and β-thymosin, each of which reduced bacterial entry upon silencing (Fig. 6) [46]. Thus,
588 one avenue for future study is to characterize the role of ADF-cofilin and other actin depolymerization
589 factors in *Chlamydia* invasion and whether dysregulation or silencing of these proteins alters the kinetics
590 of actin turnover. Furthermore, additional study is required to determine what circumstances prompt the
591 termination of actin recruitment and how *Chlamydia* achieves actin recruitment in absence of host
592 nucleators. Of particular interest is the apparent correlation between actin turnover and the presence of
593 functional TarP, TmeA, Arp2/3, and Formin 1. This raises a number of possible mechanisms that trigger
594 rapid turnover, including actin network density, physical stress that might sensitize the actin network to
595 turnover, or the actin network having a configuration that is preferred by the local depolymerization
596 machinery present.

597

598 *Divergent effects of TarP and TmeA signaling on nucleator recruitment*

599 Although we observed that both TarP and TmeA were independently capable of recruiting Arp2/3, we
600 noted that the predominant fraction of Arp2/3 recruitment was linked to TarP (Fig. 2C), while TmeA
601 signaling was associated with Arp2/3 retention within entry sites. Likewise, TarP deletion prevented
602 recruitment of Fmn1 and yielded a greater impediment to actin kinetics than TmeA deletion (Fig. 1B-E,
603 3B). Thus, our data indicate that TarP signaling is essential for nucleator collaboration, which likely occurs
604 independent of TmeA signaling. Nevertheless, our data impress the importance of TmeA signaling in
605 promoting the retention of actin nucleators and enhancing the efficiency of actin remodeling. It is unclear
606 if Arp2/3 collaborates with Fmn1 in the context of TmeA-dependent, but TarP-independent invasion and
607 actin dynamics, however available data indicate no collaboration. It may be that the actin network formed
608 by the TmeA/N-WASP/Arp2/3 axis does not offer binding sites for Fmn1, preventing any collaboration
609 from occurring. Nevertheless, our data corroborate recent findings obtained via *in vitro* pyrene-actin
610 assays which indicate that TmeA signaling through N-WASP leads to Arp2/3 activation. Within the context
611 of our model, an intriguing possibility is that TmeA signaling maintains an active pool of N-WASP to
612 activate Arp2/3 complexes bound along the length of actin filaments. However, this is speculative given
613 that we did not observe N-WASP recruitment in prior live-cell imaging experiments that lasted for 360 s
614 [9]. An added complexity is the potential involvement of growth factor receptors, e.g. EGFR, FGFR,
615 integrins, etc., which could provide the signals to activate Arp2/3, and thus would be redundant to TarP
616 and TmeA [56–60]. Besides a potential compensatory role for growth factor receptors, an additional layer
617 of complexity could come from signaling cross-talk. Given the plurality of factors involved in *Chlamydia*
618 invasion, much more research is needed to identify their individual contributions and integrate them into
619 a more comprehensive understanding of which signaling pathways influence collaboration between
620 branched and filamentous actin nucleators.

621 Although TarP signaling has not yet been definitively linked to the activation of DRFs, we identified
622 the recruitment of two DRFs, mDia1 and mDia2, which require activation by Rho-GTPases prior to serving
623 as actin nucleators or filament elongation factors. Since TarP signals through Rac1 [9,22], which is known
624 to activate mDia1 and mDia2 [61,62], our data support a model where TarP signaling contributes to the
625 assembly of both branched and filamentous actin (Figs. 2,3). Interestingly, Fmn1 recruitment was found
626 to be TarP-dependent despite the fact that Fmn1 activity, unlike DRFs, is not contingent upon activation
627 by Rho-GTPases. Fmn1 recruitment is likely mediated by the actin network nucleated by Arp2/3, with the
628 barbed ends of each branch serving as binding sites, and thus may be indirectly recruited as a product of
629 effector-mediated actin remodeling. However, since Fmn1 recruitment was absent in TarP-deficient
630 *Chlamydiae*, it seems that Arp2/3 which is activated by the alternate TmeA-dependent mechanism is
631 incapable of compensating for the recruitment of Fmn1. Thus, the means by which Arp2/3 is activated
632 appears to determine whether it will collaborate with Fmn1 during invasion. Nevertheless, the
633 recruitment of multiple formin species highlights the importance of filamentous actin polymerization
634 toward *Chlamydia* invasion, particularly since it is known that *Chlamydia* induces the assembly of
635 hypertrophic microvilli, whose assembly is reliant upon the activity of formins [63–65]. Finally, since the
636 pan-formin inhibitor SMIFH2 is expected to inhibit all three formin species identified in our study [43], we
637 are incapable of decoupling the effects of Fmn1, mDia1, and mDia2 in nucleator collaboration and
638 subsequent actin remodeling. Attempts to address the individual contributions of each formin species via
639 RNA interference were thwarted by cytotoxicity upon silencing of these proteins, preventing the use of
640 formin knockdown cells in downstream applications (i.e kinetics and invasion efficiency). Overall, our data
641 demonstrate the importance of formins toward *Chlamydia* invasion and introduce the possibility that TarP
642 signaling contributes more to actin remodeling than was previously appreciated.

643 Throughout this study, we obtained evidence that actin dynamics associated with *Chlamydia*
644 invasion have core and auxiliary elements. This is based on the correlation between the recruitment and

645 turnover phases of actin dynamics. At the population level, actin dynamics, secretion of TarP and TmeA,
646 or inhibition of either nucleators led to the reduction in the rates of recruitment and turnover. However,
647 upon detailed analysis where the recruitment phase for individual elementary bodies were matched with
648 their corresponding turnover phase, we could not demonstrate significant correlation. Elementary bodies
649 exhibiting rapid recruitment gave rise to rapid and slow turnover equally, and vice versa. When viewed
650 from the perspective of an invasion process involving core and auxiliary components, the variability at the
651 single-EB level could be accounted for by the accessory factors, which could include local concentration
652 of actin, barbed ends, depolymerizing factors, actin crosslinkers, capping, etc., while an intact core
653 component would explain the generally consistent trends observed at the population level. At the outset
654 of invasion, *Chlamydia* makes contact and subsequently activates an assortment of host receptors (EGFR,
655 PDGFR, ERα/β, β1-Integrin, etc.), which may influence the recruitment of actin, its nucleators, and actin
656 depolymerization factors (Fig. 6) [46,66,67]. Furthermore, live-cell imaging of *Chlamydia* invasion did not
657 reveal any consistent pattern of cell surface location of entry, instead occurring stochastically across the
658 surface of the cell. As such, local variations in the levels of preassembled actin filaments or the
659 concentration of signaling co-factors may exist. In addition, a myriad of other cellular machinery may be
660 differentially accessible for exploitation by *Chlamydia*. What we observed, however, is that the loss of
661 either TarP or TmeA had a substantial effect on the rate and distribution of actin kinetics, indicating that
662 TarP and TmeA are core components of invasion that expand the repertoire of signaling events by
663 coordinating the utilization of multiple accessory signaling proteins. Consequently, effector secretion
664 results in the recruitment of a cohort of proteins which influence actin dynamics and contribute to
665 efficient invasion of *C. trachomatis*, or vice versa where additional signaling events assist *Chlamydia* in
666 mediating efficient pathogen entry. In this context, EGFR, PDGFR, ERα/β, β1-Integrin and others could be
667 accessory signaling molecules that on their own are not sufficient to support efficient invasion and rapid
668 actin dynamics. This is further evidenced by the fact that deletion of either TarP or TmeA strongly

669 attenuated pathogen internalization, indicating that activation of one or more of the above receptors is
670 insufficient to compensate for loss of either effector. Instead, their functional utility only becomes
671 apparent upon secretion of TarP and/or TmeA.
672

673 **Materials and Methods:**

674 **Cell and Bacterial Culture**

675 Green monkey kidney fibroblast-like (Cos7) cells and cervical adenocarcinoma epithelial (HeLa) cells were
676 cultured at 37˚C with 5% atmospheric CO2 in Dulbecco's Modified Eagle Medium (DMEM; Gibco, Thermo
677 Fisher Scientific, Waltham, MA, USA) supplemented with 10 µg/mL gentamicin, 2 mM L-glutamine, and
678 10% (v/v) filter-sterilized fetal bovine serum (FBS). HeLa and Cos7 cells were cultured for a maximum of
679 15 passages for all experiments. McCoy B mouse fibroblasts (originally from Dr. Harlan Caldwell,
680 NIH/NIAID) were cultured under comparable conditions. *Chlamydia trachomatis* serovar L2 (434/Bu) was
681 propagated in McCoy cells and EBs were purified using a Gastrografin density gradient as described
682 previously [68].

683

684 **Reagents**

685 SMIFH2 (Tocris, Minneapolis, MN, USA) and CK666 (Sigma-Aldrich, St. Louis, MO, USA) were diluted upon
686 receipt to 100mM stock concentration in DMSO, dispensed into single-use aliquots and stored at -20°C
687 for no longer than 1 year after receipt. SMIFH2 was diluted to a working concentration of 10µM (1:10000)
688 in supplemented DMEM, and CK666 was diluted to a working concentration of 100µM (1:1000) in
689 supplemented DMEM.

690

691 **Invasion Assay**

692 Efficiency of *C. trachomatis* invasion in HeLa cells was performed as described previously [12]. Briefly,
693 HeLa cells were seeded in 24-well plates containing acid-etched glass coverslips and allowed to adhere
694 overnight. Cells were pretreated with SMIFH2 (10µM) (Tocris, Minneapolis, MN, USA), CK666 (100µM)
695 (Sigma-Aldrich, St. Louis, MO, USA), or both, for 1 hour prior to infection. Following inhibitor treatment,
696 cells were infected with EBs derived from wild-type *C. trachomatis* L2 (434/Bu), *C. trachomatis* in which

697 TarP, TmeA, or both were deleted by FRAEM (ΔTarP, ΔTmeA, ΔTmeA/ΔTarP), or *C. trachomatis* in which
698 TarP or TmeA expression was restored by *cis*-complementation (*cis*-TarP, *cis*-TmeA) at MOI=50. EBs were
699 allowed to attach to HeLa cells for 30 min at 4°C. Cells were rinsed with cold HBSS before temperature
700 shift to 37°C by the addition of pre-warmed DMEM + 10% FBS/2 mM L-glutamine and incubated at 37°C
701 for 10 min. Cells were then washed with cold HBSS containing 100 µg/mL heparin to remove any
702 transiently adherent EBs before fixation in 4% paraformaldehyde at room temperature for 15 min. Fixed
703 cells were labeled with a mouse monoclonal anti-*Chlamydia* LPS antibody (BioRad CF 6J12, Hercules, CA,
704 USA), rinsed with 1x PBS, and fixed once more in 4% paraformaldehyde for 10 min. Next, cells were
705 permeabilized using 0.1% (w/v) Triton X-100 for 10 minutes at room temperature, rinsed with HBSS and
706 labeled with rabbit polyclonal anti-*Chlamydia trachomatis* antibody (Abcam ab252762, Cambridge, MA,
707 USA). Cells were then rinsed in 1x PBS and labeled with Alexa Fluor 488 anti-mouse (ThermoFisher
708 #A28175, Waltham, MA, USA) and Alexa Fluor 594 anti-rabbit (ThermoFisher #A-11012) IgG secondary
709 antibodies. Coverslips were mounted and observed on either a Leica DM500 (Leica, Allendale, NJ, USA) or
710 Zeiss Axio Observer (Zeiss, Dublin, CA, USA) epifluorescence microscopes. Percent invasion efficiency was
711 quantified as total EBs (red) – extracellular EBs (green)/total EBs (red) x 100%.
712
713 **Quantitative live cell imaging of *Chlamydia* invasion**
714 Cos7 cells were seeded onto Ibidi µ-Slide 8-well glass-bottomed chambers (Ibidi, Fitchburg, WI, USA) and
715 allowed to adhere overnight prior to transfection. Cells were transfected with fluorescent proteins as
716 indicated, using Lipofectamine 3000 (Thermo Fisher, Waltham, MA, USA) according to manufacturer
717 directions. Transfection was allowed to proceed overnight before replacing media with fresh DMEM +
718 10% FBS/2 mM L-glutamine and allowing protein expression to continue for a total of 24 hours post-
719 transfection. Transfection was verified on either a Leica SD6000 or Nikon CSU-W1 (Nikon, Melville, NY,
720 USA) spinning disk confocal microscope prior to application of DMEM containing SMIFH2 (10µM), CK666

721 (100µM) or both. Wells were individually infected with CMTPX-labeled wild-type *C. trachomatis* L2
722 (434/Bu), unless otherwise indicated, at MOI=20 and promptly imaged using a 60x objective (NA 1.40) in
723 a heated and humidified enclosure. Images were collected once every 20 seconds for 30 minutes, with
724 focal plane maintained using an infrared auto-focusing system. Upon completion of the imaging protocol,
725 the next well was infected and imaging repeated; mock-treated wells were imaged first to allow inhibitor
726 treatment sufficient time to achieve inhibition. Images were compiled into videos using NIH ImageJ and
727 analyzed to identify protein recruitment events. The mean fluorescence intensity (MFI) of such events
728 was measured for each timepoint alongside the local background MFI of a concentric region immediately
729 outside the recruitment event. Background MFI was subtracted from recruitment MFI for each timepoint
730 and converted into fold recruitment by dividing the MFI of each timepoint against the baseline MFI,
731 defined as the average MFI of five timepoints (100 sec) prior to the start of recruitment.
732
733 **Plasmids and DNA preparation**
734 pEGFP-Actin–C1 [69] was provided by Dr Scott Grieshaber (University of Idaho). pEGFP-N1-ACTR3 (Arp3-
735 GFP) [47] was obtained from Dr Matthew Welch (Addgene plasmid #8462). Arp3-pmCherryC1 [70] was a
736 gift from Christien Merrifield (Addgene plasmid #27682). mEmerald-mDia1-N-14 (Addgene plasmid
737 #54157), mEmerald-mDia2-N-14 (Addgene plasmid #54159), and mRuby-LifeAct-7 (Addgene plasmid
738 #54560) were gifted by Michael Davidson. pEGFPC2-FmnIso1b [71] was a gift from Philip Leder (Addgene
739 plasmid #19320). pmCherryC1-FmnIso1b was generated by a variant of Gibson assembly termed
740 FastCloning [72] and included removal of EGFP from pEGFPC2-FmnIso1b and insertion of mCherry derived
741 from Arp3-pmCherryC1. Kanamycin-resistant transformants were selected and propagated for plasmid
742 isolation prior to sequence verification using an mCherry-Fwd sequencing primer supplied by Eurofins
743 Genomics. All plasmids were isolated using MiniPrep DNA isolation kits (Qiagen, Valencia, CA, USA)
744 following a variant protocol for DNA isolation termed MiraPrep [73]. Following plasmid isolation, the

745 eluate was precipitated by addition of 3M sodium acetate (Invitrogen, Waltham, MA, USA) at 10% (v/v)
746 of eluate volume followed by addition of 250% (v/v) absolute ethanol calculated after addition of sodium
747 acetate. The mixture was incubated at 4°C overnight and centrifuged at 14,000×g for 15 minutes at 4°C.
748 Supernatant was removed and 70% ethanol was added, followed by centrifugation at 14,000×g for 10
749 minutes at 4°C. Supernatant was removed once more, and precipitated DNA was resuspended in
750 nuclease-free H_2O. Primers for assembly of pmCherryC1-FmnIso1b are as follows: (pEGFPC2) Fwd: 5'
751 GGCGGAAGCGGAAGCATGGAAGGCACTCACTGCACC 3', Rev: 5' GCCCTTGCTCACCAT
752 GGTGGCGACCGGTAGCG 3'; (pmCherryC1) Fwd: 5' CTACCGGTCGCCACCATGGTGAGCAAGGGCGAGG 3',
753 Rev: 5' GTGAGTGCCTTCCATGCTTCCGCTTCCGCCG 3'.
754
755 **Graphs and statistical analysis**
756 Violin plots were made using the ggplot2 base package (version 3.1.0) as a component of the Tidyverse
757 package (https://cran.r-project.org/web/packages/tidyverse/index.html) in rStudio (version 4.0.3).
758 Wilcoxon ranked-sum tests to determine statistical significance between violin plots and tabulated
759 statistical analyses of violin plots were generated using base R statistics and the moments package
760 (version 0.14, https://cran.r-project.org/web/packages/moments/index.html) in rStudio and assembled
761 in Excel (Microsoft, Redmond, WA, USA). Linear regression analyses, recruitment plots, invasion assays,
762 and all statistics associated with these data (pairwise T-test, correlation coefficient, SEM) were performed
763 in Excel. All graphs were assembled using the free and open-source software GNU Image Manipulation
764 Program (GIMP, https://www.gimp.org/) and Inkscape (https://inkscape.org/). Proposed model for
765 collaboration (Fig. 6) was assembled using BioRender (https://app.biorender.com/).
766

767 **Acknowledgements**

768 We thank the members of the Carabeo lab for extensive feedback regarding the design, direction, and
769 analysis of the study. We thank Dr. Ken Fields (University of Kentucky College of Medicine) for the kind
770 gift of ΔTarP, ΔTmeA, ΔTmeA/ΔTarP and TarP/TmeA *cis*-complemented strains. This study was supported
771 by funding from the U.S. National Institutes of Health, National Institutes of Allergy and Infectious Disease
772 grant R01 AI065545 (R.A.C.). M.D.R. was further supported by a fellowship from the Seattle Chapter of
773 Achievement Rewards for College Scientists (ARCS). The contents and views expressed within this
774 publication are the sole responsibility of the authors.

775

776 **Author Contributions:**

777 M.D.R. and R.A.C. designed the experiments and wrote the manuscript. M.D.R. performed the
778 experiments, and M.D.R. and R.A.C. analyzed the data.

779

780 **Conflict of Interest**

781 The authors declare no conflict of interest.

782

783 **Data Availability**

784 Datasets regarding the raw data and analysis of invasion assays, fluorescence microscopy and associated
785 kinetic analyses are available in Dryad (https://doi.org/10.5061/dryad.0k6djhb0g).

786

787 **References:**

788 1. Malhotra M, Sood S, Mukherjee A, Muralidhar S, Bala M. Genital Chlamydia trachomatis: An update.
789 Indian J Med Res. 2013;138: 303–316.

790 2. Bastidas RJ, Elwell CA, Engel JN, Valdivia RH. Chlamydial intracellular survival strategies. Cold Spring
791 Harb Perspect Med. 2013;3: a010256. doi:10.1101/cshperspect.a010256

792 3. Su H, Raymond L, Rockey DD, Fischer E, Hackstadt T, Caldwell HD. A recombinant Chlamydia
793 trachomatis major outer membrane protein binds to heparan sulfate receptors on epithelial cells.
794 Proc Natl Acad Sci U S A. 1996;93: 11143–11148. doi:10.1073/pnas.93.20.11143

795 4. Zhang JP, Stephens RS. Mechanism of C. trachomatis attachment to eukaryotic host cells. Cell.
796 1992;69: 861–869. doi:10.1016/0092-8674(92)90296-o

797 5. Gitsels A, Sanders N, Vanrompay D. Chlamydial Infection From Outside to Inside. Front Microbiol.
798 2019;10. doi:10.3389/fmicb.2019.02329

799 6. Fields KA, Mead DJ, Dooley CA, Hackstadt T. Chlamydia trachomatis type III secretion: evidence for
800 a functional apparatus during early-cycle development. Mol Microbiol. 2003;48: 671–683.
801 doi:10.1046/j.1365-2958.2003.03462.x

802 7. Chen Y-S, Bastidas RJ, Saka HA, Carpenter VK, Richards KL, Plano GV, et al. The Chlamydia
803 trachomatis type III secretion chaperone Slc1 engages multiple early effectors, including TepP, a
804 tyrosine-phosphorylated protein required for the recruitment of CrkI-II to nascent inclusions and
805 innate immune signaling. PLoS Pathog. 2014;10: e1003954. doi:10.1371/journal.ppat.1003954

806 8. Thwaites TR, Pedrosa AT, Peacock TP, Carabeo RA. Vinculin Interacts with the Chlamydia Effector
807 TarP Via a Tripartite Vinculin Binding Domain to Mediate Actin Recruitment and Assembly at the
808 Plasma Membrane. Front Cell Infect Microbiol. 2015;5. doi:10.3389/fcimb.2015.00088

809 9. Carabeo RA, Dooley CA, Grieshaber SS, Hackstadt T. Rac interacts with Abi-1 and WAVE2 to promote
810 an Arp2/3-dependent actin recruitment during chlamydial invasion. Cellular Microbiology. 2007;9:
811 2278–2288. doi:https://doi.org/10.1111/j.1462-5822.2007.00958.x

812 10. Fadel S, Eley A. Differential glycosaminoglycan binding of Chlamydia trachomatis OmcB protein from
813 serovars E and LGV. J Med Microbiol. 2008;57: 1058–1061. doi:10.1099/jmm.0.2008/001305-0

814 11. Hower S, Wolf K, Fields KA. Evidence that CT694 is a novel Chlamydia trachomatis T3S substrate
815 capable of functioning during invasion or early cycle development. Mol Microbiol. 2009;72: 1423–
816 1437. doi:10.1111/j.1365-2958.2009.06732.x

817 12. Carabeo RA, Grieshaber SS, Fischer E, Hackstadt T. Chlamydia trachomatis Induces Remodeling of
818 the Actin Cytoskeleton during Attachment and Entry into HeLa Cells. Infect Immun. 2002;70: 3793–
819 3803. doi:10.1128/IAI.70.7.3793-3803.2002

820 13. Caven L, Carabeo RA. Pathogenic Puppetry: Manipulation of the Host Actin Cytoskeleton by
821 Chlamydia Trachomatis. 2019 [cited 3 Apr 2020]. Available:
822 https://www.preprints.org/manuscript/201912.0113/v1

823 14. Ford C, Nans A, Boucrot E, Hayward RD. Chlamydia exploits filopodial capture and a
824 macropinocytosis-like pathway for host cell entry. PLOS Pathogens. 2018;14: e1007051.
825 doi:10.1371/journal.ppat.1007051

826 15. Francis CL, Ryan TA, Jones BD, Smith SJ, Falkow S. Ruffles induced by Salmonella and other stimuli
827 direct macropinocytosis of bacteria. Nature. 1993;364: 639–642. doi:10.1038/364639a0

828 16. Zhou D, Mooseker MS, Galán JE. An invasion-associated Salmonella protein modulates the actin-
829 bundling activity of plastin. PNAS. 1999;96: 10176–10181. doi:10.1073/pnas.96.18.10176

830 17. Reed SCO, Lamason RL, Risca VI, Abernathy E, Welch MD. Rickettsia Actin-Based Motility Occurs in
831 Distinct Phases Mediated by Different Actin Nucleators. Current Biology. 2014;24: 98–103.
832 doi:10.1016/j.cub.2013.11.025

833 18. Carabeo RA, Grieshaber SS, Hasenkrug A, Dooley C, Hackstadt T. Requirement for the Rac GTPase in
834 Chlamydia trachomatis invasion of non-phagocytic cells. Traffic. 2004;5: 418–425.
835 doi:10.1111/j.1398-9219.2004.00184.x

836 19. Bailly M, Macaluso F, Cammer M, Chan A, Segall JE, Condeelis JS. Relationship between Arp2/3
837 Complex and the Barbed Ends of Actin Filaments at the Leading Edge of Carcinoma Cells after
838 Epidermal Growth Factor Stimulation. J Cell Biol. 1999;145: 331–345.

839 20. Mullins RD, Heuser JA, Pollard TD. The interaction of Arp2/3 complex with actin: Nucleation, high
840 affinity pointed end capping, and formation of branching networks of filaments. PNAS. 1998;95:
841 6181–6186. doi:10.1073/pnas.95.11.6181

842 21. Higgs HN, Pollard TD. Regulation of Actin Polymerization by Arp2/3 Complex and WASp/Scar
843 Proteins *. Journal of Biological Chemistry. 1999;274: 32531–32534. doi:10.1074/jbc.274.46.32531

844 22. Lane BJ, Mutchler C, Al Khodor S, Grieshaber SS, Carabeo RA. Chlamydial Entry Involves TARP Binding
845 of Guanine Nucleotide Exchange Factors. PLOS Pathogens. 2008;4: e1000014.
846 doi:10.1371/journal.ppat.1000014

847 23. Faris R, McCullough A, Andersen SE, Moninger TO, Weber MM. The Chlamydia trachomatis secreted
848 effector TmeA hijacks the N-WASP-ARP2/3 actin remodeling axis to facilitate cellular invasion. PLOS
849 Pathogens. 2020;16: e1008878. doi:10.1371/journal.ppat.1008878

850 24. Keb G, Ferrell J, Scanlon KR, Jewett TJ, Fields KA. Chlamydia trachomatis TmeA Directly Activates N-
851 WASP To Promote Actin Polymerization and Functions Synergistically with TarP during Invasion.
852 mBio. 2021;12: e02861-20. doi:10.1128/mBio.02861-20

853 25. Shemesh T, Kozlov MM. Actin Polymerization upon Processive Capping by Formin: A Model for
854 Slowing and Acceleration. Biophys J. 2007;92: 1512–1521. doi:10.1529/biophysj.106.098459

855 26. Yang C, Czech L, Gerboth S, Kojima S, Scita G, Svitkina T. Novel roles of formin mDia2 in lamellipodia
856 and filopodia formation in motile cells. PLoS Biol. 2007;5: e317. doi:10.1371/journal.pbio.0050317

857 27. Kage F, Winterhoff M, Dimchev V, Mueller J, Thalheim T, Freise A, et al. FMNL formins boost
858 lamellipodial force generation. Nat Commun. 2017;8: 14832. doi:10.1038/ncomms14832

859 28. Fattouh R, Kwon H, Czuczman MA, Copeland JW, Pelletier L, Quinlan ME, et al. The Diaphanous-
860 Related Formins Promote Protrusion Formation and Cell-to-Cell Spread of Listeria monocytogenes.
861 The Journal of Infectious Diseases. 2015;211: 1185–1195. doi:10.1093/infdis/jiu546

862 29. Baarlink C, Brandt D, Grosse R. SnapShot: Formins. Cell. 2010;142: 172, 172.e1.
863 doi:10.1016/j.cell.2010.06.030

864 30. Rengarajan M, Hayer A, Theriot JA. Endothelial Cells Use a Formin-Dependent Phagocytosis-Like
865 Process to Internalize the Bacterium Listeria monocytogenes. PLOS Pathogens. 2016;12: e1005603.
866 doi:10.1371/journal.ppat.1005603

867 31. Boddy KC, Gao AD, Truong D, Kim MS, Froese CD, Trimble WS, et al. Septin-regulated actin dynamics
868 promote Salmonella invasion of host cells. Cell Microbiol. 2018;20. doi:10.1111/cmi.12866

869 32. Williams SK, Weiner ZP, Gilmore RD. Human neuroglial cells internalize Borrelia burgdorferi by
870 coiling phagocytosis mediated by Daam1. PLoS One. 2018;13: e0197413.
871 doi:10.1371/journal.pone.0197413

872 33. Rotty JD, Bear JE. Competition and collaboration between different actin assembly pathways allows
873 for homeostatic control of the actin cytoskeleton. Bioarchitecture. 2015;5: 27–34.
874 doi:10.1080/19490992.2015.1090670

875 34. Swaney KF, Li R. Function and regulation of the Arp2/3 complex during cell migration in diverse
876 environments. Curr Opin Cell Biol. 2016;42: 63–72. doi:10.1016/j.ceb.2016.04.005

877 35. Isogai T, Kammen R van der, Leyton-Puig D, Kedziora KM, Jalink K, Innocenti M. Initiation of
878 lamellipodia and ruffles involves cooperation between mDia1 and the Arp2/3 complex. J Cell Sci.
879 2015;128: 3796–3810. doi:10.1242/jcs.176768

880 36. Naj X, Hoffmann A-K, Himmel M, Linder S. The Formins FMNL1 and mDia1 Regulate Coiling
881 Phagocytosis of Borrelia burgdorferi by Primary Human Macrophages. Infection and Immunity.
882 2013;81: 1683–1695. doi:10.1128/IAI.01411-12

883 37. Velle KB, Campellone KG. Enteropathogenic E. coli relies on collaboration between the formin mDia1
884 and the Arp2/3 complex for actin pedestal biogenesis and maintenance. PLoS Pathog. 2018;14:
885 e1007485. doi:10.1371/journal.ppat.1007485

886 38. Brieher W. Mechanisms of actin disassembly. MBoC. 2013;24: 2299–2302. doi:10.1091/mbc.e12-
887 09-0694

888 39. Carlier M-F, Shekhar S. Global treadmilling coordinates actin turnover and controls the size of actin
889 networks. Nature Reviews Molecular Cell Biology. 2017;18: 389–401. doi:10.1038/nrm.2016.172

890 40. Zheng K, Kitazato K, Wang Y, He Z. Pathogenic microbes manipulate cofilin activity to subvert actin
891 cytoskeleton. Critical Reviews in Microbiology. 2016;42: 677–695.
892 doi:10.3109/1040841X.2015.1010139

893 41. Zrieq R, Braun C, Hegemann JH. The Chlamydia pneumoniae Tarp Ortholog CPn0572 Stabilizes Host
894 F-Actin by Displacement of Cofilin. Front Cell Infect Microbiol. 2017;7.
895 doi:10.3389/fcimb.2017.00511

896 42. Jiwani S, Ohr RJ, Fischer ER, Hackstadt T, Alvarado S, Romero A, et al. Chlamydia trachomatis Tarp
897 cooperates with the Arp2/3 complex to increase the rate of actin polymerization. Biochem Biophys
898 Res Commun. 2012;420: 816–821. doi:10.1016/j.bbrc.2012.03.080

899 43. Rizvi SA, Neidt EM, Cui J, Feiger Z, Skau CT, Gardel ML, et al. Identification and characterization of a
900 small molecule inhibitor of formin-mediated actin assembly. Chem Biol. 2009;16: 1158–1168.
901 doi:10.1016/j.chembiol.2009.10.006

902 44. Nishimura Y, Shi S, Zhang F, Liu R, Takagi Y, Bershadsky AD, et al. The formin inhibitor SMIFH2 inhibits
903 members of the myosin superfamily. J Cell Sci. 2021;134: jcs253708. doi:10.1242/jcs.253708

904 45. Hetrick B, Han MS, Helgeson LA, Nolen BJ. Small molecules CK-666 and CK-869 inhibit Arp2/3
905 complex by blocking an activating conformational change. Chem Biol. 2013;20: 701–712.
906 doi:10.1016/j.chembiol.2013.03.019

907 46. Elwell CA, Ceesay A, Kim JH, Kalman D, Engel JN. RNA Interference Screen Identifies Abl Kinase and
908 PDGFR Signaling in Chlamydia trachomatis Entry. PLOS Pathogens. 2008;4: e1000021.
909 doi:10.1371/journal.ppat.1000021

910 47. Welch MD, DePace AH, Verma S, Iwamatsu A, Mitchison TJ. The Human Arp2/3 Complex Is
911 Composed of Evolutionarily Conserved Subunits and Is Localized to Cellular Regions of Dynamic Actin
912 Filament Assembly. J Cell Biol. 1997;138: 375–384.

913 48. Meconi S, Jacomo V, Boquet P, Raoult D, Mege J-L, Capo C. Coxiella burnetii Induces Reorganization
914 of the Actin Cytoskeleton in Human Monocytes. Infection and Immunity. 1998;66: 5527–5533.
915 doi:10.1128/IAI.66.11.5527-5533.1998

916 49. Elwell C, Mirrashidi K, Engel J. Chlamydia cell biology and pathogenesis. Nature Reviews
917 Microbiology. 2016;14: 385–400. doi:10.1038/nrmicro.2016.30

918 50. Jewett TJ, Fischer ER, Mead DJ, Hackstadt T. Chlamydial TARP is a bacterial nucleator of actin. Proc
919 Natl Acad Sci U S A. 2006;103: 15599–15604. doi:10.1073/pnas.0603044103

920 51. Dai S, Sarmiere PD, Wiggan O, Bamburg JR, Zhou D. Efficient Salmonella entry requires activity cycles
921 of host ADF and cofilin. Cell Microbiol. 2004;6: 459–471. doi:10.1111/j.1462-5822.2004.00375.x

922 52. Bierne H, Gouin E, Roux P, Caroni P, Yin HL, Cossart P. A role for cofilin and LIM kinase in Listeria-
923 induced phagocytosis. J Cell Biol. 2001;155: 101–112. doi:10.1083/jcb.200104037

924 53. Moffatt CE, Inaba H, Hirano T, Lamont RJ. Porphyromonas gingivalis SerB-mediated
925 dephosphorylation of host cell cofilin modulates invasion efficiency. Cellular Microbiology. 2012;14:
926 577–588. doi:https://doi.org/10.1111/j.1462-5822.2011.01743.x

927 54. Maldonado-Contreras A, Birtley JR, Boll E, Zhao Y, Mumy KL, Toscano J, et al. Shigella depends on
928 SepA to destabilize the intestinal epithelial integrity via cofilin activation. Gut Microbes. 2017;8:
929 544–560. doi:10.1080/19490976.2017.1339006

930 55. Pieters J, Müller P, Jayachandran R. On guard: coronin proteins in innate and adaptive immunity.
931 Nature Reviews Immunology. 2013;13: 510–518. doi:10.1038/nri3465

932 56. Sah P, Lutter EI. Hijacking and Use of Host Kinases by Chlamydiae. Pathogens. 2020;9: E1034.
933 doi:10.3390/pathogens9121034

934 57. Mölleken K, Becker E, Hegemann JH. The Chlamydia pneumoniae invasin protein Pmp21 recruits the
935 EGF receptor for host cell entry. PLoS Pathog. 2013;9: e1003325. doi:10.1371/journal.ppat.1003325

936 58. Kim JH, Jiang S, Elwell CA, Engel JN. Chlamydia trachomatis Co-opts the FGF2 Signaling Pathway to
937 Enhance Infection. Valdivia RH, editor. PLoS Pathogens. 2011;7: e1002285.
938 doi:10.1371/journal.ppat.1002285

939 59. Patel AL, Chen X, Wood ST, Stuart ES, Arcaro KF, Molina DP, et al. Activation of epidermal growth
940 factor receptor is required for Chlamydia trachomatis development. BMC Microbiol. 2014;14: 277.
941 doi:10.1186/s12866-014-0277-4

942 60. Stallmann S, Hegemann JH. The Chlamydia trachomatis Ctad1 invasin exploits the human integrin
943 β1 receptor for host cell entry. Cellular Microbiology. 2016;18: 761–775. doi:10.1111/cmi.12549

944 61. Lammers M, Meyer S, Kühlmann D, Wittinghofer A. Specificity of Interactions between mDia
945 Isoforms and Rho Proteins. J Biol Chem. 2008;283: 35236–35246. doi:10.1074/jbc.M805634200

946 62. Ji P, Jayapal SR, Lodish HF. Enucleation of cultured mouse fetal erythroblasts requires Rac GTPases
947 and mDia2. Nat Cell Biol. 2008;10: 314–321. doi:10.1038/ncb1693

948 63. Harris ES, Gauvin TJ, Heimsath EG, Higgs HN. Assembly of filopodia by the formin FRL2 (FMNL3).
949 Cytoskeleton. 2010;67: 755–772. doi:https://doi.org/10.1002/cm.20485

950 64. Huang C-R, Kuo C-J, Huang C-W, Chen Y-T, Liu B-Y, Lee C-T, et al. Host CDK-1 and formin mediate
951 microvillar effacement induced by enterohemorrhagic Escherichia coli. Nature Communications.
952 2021;12: 90. doi:10.1038/s41467-020-20355-1

953 65. Pelaseyed T, Bretscher A. Regulation of actin-based apical structures on epithelial cells. J Cell Sci.
954 2018;131. doi:10.1242/jcs.221853

955 66. Stallmann S, Hegemann JH. The Chlamydia trachomatis Ctad1 invasin exploits the human integrin
956 β1 receptor for host cell entry. Cell Microbiol. 2016;18: 761–775. doi:10.1111/cmi.12549

957 67. Davis CH, Raulston JE, Wyrick PB. Protein Disulfide Isomerase, a Component of the Estrogen
958 Receptor Complex, Is Associated with Chlamydia trachomatis Serovar E Attached to Human

959 Endometrial Epithelial Cells. Infect Immun. 2002;70: 3413–3418. doi:10.1128/IAI.70.7.3413-
960 3418.2002

961 68. Caldwell HD, Kromhout J, Schachter J. Purification and partial characterization of the major outer
962 membrane protein of Chlamydia trachomatis. Infect Immun. 1981;31: 1161–1176.
963 doi:10.1128/IAI.31.3.1161-1176.1981

964 69. Heinzen RA, Grieshaber SS, Van Kirk LS, Devin CJ. Dynamics of Actin-Based Movement by Rickettsia
965 rickettsii in Vero Cells. Infect Immun. 1999;67: 4201–4207.

966 70. Taylor MJ, Perrais D, Merrifield CJ. A high precision survey of the molecular dynamics of mammalian
967 clathrin-mediated endocytosis. PLoS Biol. 2011;9: e1000604. doi:10.1371/journal.pbio.1000604

968 71. Zhou F, Leder P, Martin SS. Formin-1 protein associates with microtubules through a peptide domain
969 encoded by exon-2. Exp Cell Res. 2006;312: 1119–1126. doi:10.1016/j.yexcr.2005.12.035

970 72. Li C, Wen A, Shen B, Lu J, Huang Y, Chang Y. FastCloning: a highly simplified, purification-free,
971 sequence- and ligation-independent PCR cloning method. BMC Biotechnology. 2011;11: 92.
972 doi:10.1186/1472-6750-11-92

973 73. Pronobis MI, Deuitch N, Peifer M. The Miraprep: A Protocol that Uses a Miniprep Kit and Provides
974 Maxiprep Yields. PLOS ONE. 2016;11: e0160509. doi:10.1371/journal.pone.0160509

975

976 **Figure 1: Deletion of TarP and TmeA impair invasion and attenuates kinetics of actin recruitment and**
977 **turnover.**
978 (A,B) Cos7 cells were transfected with Actin-GFP or mRuby-LifeAct for 24 hours prior to infection with
979 wild-type, single-knockout (ΔTarP, ΔTmeA), cis-complemented (*cis*-TarP, *cis*-TmeA), or double-knockout
980 (ΔTmeA/ΔTarP) *Chlamydia* strains at MOI=20. Infection was monitored by live-cell confocal microscopy
981 using a Nikon CSU-W1 spinning disk microscope, obtaining images every 20 seconds for 30 minutes to
982 identify sites exhibiting actin recruitment. (B) Recruitment events were isolated by selecting regions
983 containing invading *Chlamydia* and elevated actin fluorescence. Background fluorescence was subtracted,
984 and fold recruitment was calculated as a function of the fold increase in mean fluorescence intensity of
985 recruited actin compared to basal actin fluorescence. Detailed visualization of this process can be found
986 in Fig. S1. Data is displayed as mean fold recruitment for each timepoint +/- SEM compiled from a
987 minimum N=18 recruitment events. (C) HeLa cells were infected with each *Chlamydia* strain indicated
988 above at MOI=50 and stained using the "in-and-out" method which distinguishes non-internalized EBs
989 from total cell-associated EBs, as described in Materials and Methods. Results were normalized against
990 mean invasion efficiency of wild-type *Chlamydia* and plotted as normalized mean +/- SEM. Data was
991 collected from 15 fields, with each field containing an average of 100 *Chlamydiae*. Statistical significance
992 was determined by T- test. (D,E) All actin recruitment events used to create the averaged plot shown
993 previously (Fig. 1B) were individually divided into recruitment and turnover phases (Fig. S2). Individual
994 rates of (D) recruitment and (E) turnover were plotted on a violin plot with inset boxplot, reporting the
995 median rate +/- SD for each strain tested. Violin plots contain a minimum N=18 individual rates. Statistical
996 significance was determined by Wilcoxon Rank-sum. All data are representative of at least 3 independent
997 experiments, * $P \leq 0.05$, ** $P \leq 0.01$, *** $P \leq 0.001$.
998
999 **Figure 2: Deletion of TarP and TmeA exerts divergent effects on Arp2/3 kinetics.**

1000 (A,B) Cos7 cells were transfected with Arp3-GFP or Arp3-mCherry for 24 hours prior to infection with wild-
1001 type, single-knockout (ΔTarP, ΔTmeA), cis-complemented (*cis*-TarP, *cis*-TmeA), or double-knockout
1002 (ΔTmeA/ΔTarP) *Chlamydia* strains at MOI=20. Infection was monitored by live-cell confocal microscopy
1003 using a Nikon CSU-W1 spinning disk microscope, obtaining images every 20 seconds for 30 minutes to
1004 identify sites exhibiting Arp3 recruitment. (B) Fluorescence intensity of Arp3 recruitment was measured
1005 as described earlier (Fig. 1B) and plotted as mean fold recruitment for each timepoint +/- SEM compiled
1006 from a minimum N=12 recruitment events. (C,D) Kinetics of Arp3 recruitment and turnover were analyzed
1007 for each strain indicated above using the same methodology described in Fig. 1D,E. Violin plots contain a
1008 minimum N=12 individual rates, reporting the median rate +/- SD. Statistical significance was determined
1009 by Wilcoxon Rank-sum. All data are representative of at least 3 independent experiments, * $P \leq 0.05$, **
1010 $P \leq 0.01$, *** $P \leq 0.001$.
1011
1012 **Figure 3: Deletion of TarP prevents recruitment of Fmn1 during invasion**
1013 (A,B) Cos7 cells were transfected with formin 1 isoform 1B fused to GFP (Fmn1-GFP) or mCherry (Fmn1-
1014 mCherry) for 24 hours prior to infection with wild-type, single-knockout (ΔTarP, ΔTmeA), cis-
1015 complemented (*cis*-TarP, *cis*-TmeA), or double-knockout (ΔTmeA/ΔTarP) *Chlamydia* strains at MOI=20.
1016 Infection was monitored by live-cell confocal microscopy using a Nikon CSU-W1 spinning disk microscope,
1017 obtaining images every 20 seconds for 30 minutes to identify sites exhibiting Fmn1 recruitment. (B)
1018 Fluorescence intensity of Fmn1 recruitment was measured as described earlier (Fig. 1B) and plotted as
1019 mean fold recruitment for each timepoint +/- SEM compiled from a minimum N=15 recruitment events.
1020 (C,D) Kinetics of Fmn1 recruitment and turnover were analyzed for each strain indicated above using the
1021 same methodology described in Fig. 1D,E. Violin plots contain a minimum N=15 individual rates, reporting
1022 the median rate +/- SD. Statistical significance was determined by Wilcoxon Rank-sum. All data are
1023 representative of at least 3 independent experiments, * $P \leq 0.05$, ** $P \leq 0.01$, *** $P \leq 0.001$.

1024

1025 **Figure 4. Formin and Arp2/3 activity are necessary for efficient invasion and optimal actin recruitment**

1026 **kinetics.**

1027 (A) Cos7 cells were transfected with GFP-Fmn1, mEmerald-mDia1, or mEmerald-mDia2 for 24hrs prior to

1028 infection with *Chlamydia* stained with CMTPX at MOI=20. Infection was monitored by live-cell confocal

1029 microscopy using a Leica SD6000 AF Spinning Disc microscope with a 60x (NA 1.40) objective. Images were

1030 obtained every 20 seconds for 30 minutes and compiled into videos in ImageJ to identify sites exhibiting

1031 colocalization of host formins (GFP) and *Chlamydia* (RFP). (B) HeLa cells were mock-treated or pretreated

1032 with inhibitors against formin (10µM SMIFH2), Arp2/3 (100µM CK666) or both (CK+SMI) for 1hr, infected

1033 with *C. trachomatis* serovar L2 at MOI=50 and stained using the "in-and-out" method which distinguishes

1034 non-internalized EBs from total cell-associated EBs, as described in Materials and Methods. Results were

1035 normalized against mean invasion efficiency of mock treated cells (Untreated mean = 49% invasion

1036 efficiency) and plotted as normalized mean +/- SEM. Data was collected from 20 fields, with each field

1037 containing an average of 108 Chlamydiae. Statistical significance was determined by T- test. (C) Cos7 cells

1038 were transfected with GFP-actin or a GFP empty vector plasmid for 24hrs prior to mock-treatment or

1039 pretreatment with 10µM SMIFH2, 100µM CK666, or both for 1hr. Transfected cells were infected with

1040 *Chlamydia* stained with CMTPX at MOI=20 and imaged by quantitative live-cell imaging, collecting images

1041 every 20 seconds for 30 minutes. Fluorescence intensity of GFP-actin recruitment was measured as

1042 described earlier (Fig. 1B) and plotted as mean fold recruitment for each timepoint +/- SEM compiled from

1043 a minimum N=16 recruitment events. (D,E) Kinetics of GFP-actin recruitment and turnover were analyzed

1044 for each condition using the same methodology described in Fig. 1D,E. Violin plots contain a minimum

1045 N=16 individual rates, reporting the median rate +/- SD. Statistical significance was determined by

1046 Wilcoxon Rank-sum. All data are representative of at least 3 independent experiments, * $P \leq 0.05$, ** $P \leq$

1047 0.01, *** $P \leq 0.001$.

1048

1049 **Figure 5: Formin 1 and Arp3 collaboration enhances recruitment kinetics at entry sites.**

1050 (A,B) Cos7 cells were transfected with (A) GFP-formin 1 isoform 1B (GFP-Fmn1) or (B) GFP-Arp3 for 24
1051 hours prior to mock-treatment or pretreatment with 10µM SMIFH2 or 100µM CK666 for 1 hour.
1052 Quantitative live-cell imaging of invading CMTPX- labeled *Chlamydia* (MOI=20) was performed as
1053 described in Fig. 1B. Briefly, images were acquired once every 20 seconds for 30 minutes and assembled
1054 into videos. MFI of recruitment events were obtained, and background fluorescence subtracted, before
1055 quantifying and plotting the fold recruitment values +/- SEM of Fmn1 or Arp3 for each timepoint. Data
1056 was compiled from a minimum N=16 recruitment events. (C) Cos7 cells were co-transfected with GFP-
1057 Fmn1 and mCherry-Arp3 for 24 hours prior to infection with unlabeled *C. trachomatis* (MOI=20) followed
1058 by quantitative live-cell imaging of invasion. Image acquisition and processing was performed as described
1059 above with a few modifications. Since CMTPX and mCherry-Arp3 fluorescence overlap, unlabeled
1060 *Chlamydia* was used, thus recruitment events are defined simply as regions containing elevated GFP-Fmn1
1061 fluorescence compared to local background. MFI of both GFP-Fmn1 and mCherry-Arp3 were obtained
1062 from the recruitment ROI, and background was subtracted from both GFP and RFP channels
1063 independently. Maximal MFI was derived from both channels and used to normalize fluorescence as
1064 percent maximal MFI for each protein. Normalized MFI values for each timepoint were compiled from 33
1065 events, plotting mean %Max MFI +/- SEM. (D) Recruitment of mEmerald-mDia1 and mEmerald-mDia2 was
1066 monitored in the presence and absence of 100µM CK666 using the method described above for
1067 monitoring the recruitment of GFP-Fmn1 and GFP-Arp3. Data is displayed as mean fold recruitment for
1068 each timepoint +/- SEM compiled from a minimum N=22 recruitment events. (E,F) Kinetics of Fmn1 and
1069 Arp3 recruitment and turnover were analyzed in the presence and absence of 100µM CK666 or 10µM
1070 SMIFH2, respectively, using the same methodology described in Fig. 1D,E. Violin plots contain a minimum
1071 N=16 individual rates, reporting the median rate +/- SD. Statistical significance was determined by

1072 Wilcoxon Rank-sum. All data are representative of at least 3 independent experiments, * $P \leq 0.05$, ** $P \leq$
1073 0.01, *** $P \leq 0.001$.
1074
1075 **Figure 6: Proposed model for collaboration between formin and Arp2/3 and subsequent rapid actin**
1076 **recruitment and turnover.**
1077 *C. trachomatis* engages and activates a multitude of host receptors whose activation is linked to the
1078 recruitment of formin, Arp2/3, and actin in non-invasion contexts. It is currently unknown whether
1079 receptor activation contributes to actin remodeling during invasion. Concurrent with receptor
1080 engagement, *Chlamydia* secretes the effectors TmeA and TarP via Type III secretion system; each effector
1081 activates Arp2/3 through N-WASP or WAVE2, respectively. Deletion of either TarP or TmeA attenuated
1082 the kinetics of Arp2/3 recruitment and turnover, which may reflect a failure to optimally activate and
1083 integrate Arp2/3 into actin networks. In addition to recruiting Arp2/3, TarP was also shown to be essential
1084 for the recruitment of Fmn1 and may also function to recruit mDia1 and/or mDia2 via signaling through
1085 Rac1. Collaboration between Arp2/3 and formin via their respective actin branching and elongating
1086 activities increases the rate of actin recruitment. Inhibition of Arp2/3 by CK666 or formin by SMIFH2
1087 prevents this collaboration and constrains the actin network into either filamentous-only or branching-
1088 only networks. The actin network generated by *Chlamydia* is rapidly turned over alongside the actin
1089 nucleators found within it. Although the precise mechanism by which this process occurs remains
1090 unknown, several actin depolymerization factors, including ADF/Cofilin, have been implicated by an siRNA
1091 screen to participate in invasion.
1092

1093 **Figure S1: Detailed image analysis throughput used to evaluate the intensity of protein recruitment.**
1094 Quantitative live-cell imaging of fluorescent protein recruitment was utilized several times in various
1095 conditions throughout this study, necessitating a consistent throughput to facilitate direct comparison.
1096 (A) Videos of *Chlamydia* invasion were assembled following image acquisition in ImageJ and analyzed to
1097 identify protein recruitment events. Protein recruitment was defined by regions exhibiting high
1098 fluorescence intensity (Yellow) as compared to local background (Red). When possible, fluorescent
1099 *Chlamydia* (CMTPX-*Chlamydia,* GFP-*Chlamydia,* RFP-*Chlamydia*) were used to ensure recruitment was
1100 specific to an invading bacterium. Regions-of-interest (ROIs) specific to recruitment were selected to
1101 include the entirety of the recruitment event across all timepoints, and a concentric region immediately
1102 outside of this region was selected as a background ROI. (B) The mean fluorescence intensity (MFI) of both
1103 recruitment and background ROI was obtained for each timepoint. (C) Background MFI was subtracted
1104 from recruitment MFI to normalize for local variations in fluorescence intensity and for photobleaching
1105 during image acquisition. Fold recruitment was calculated by dividing the MFI of each timepoint by the
1106 average MFI of 5 timepoints (100 sec, yellow dots) prior to the start of recruitment, defined as the point
1107 in which recruitment velocity begins to increase. (D) Fold recruitment values were plotted against time
1108 for each recruitment event. Multiple events were aligned according to peak recruitment for each event
1109 before calculating the mean fold recruitment across all events.

1110

1111 **Figure S2: Entry and exit points for each phase determined by velocity of recruitment and turnover.**
1112 Each event used to generate the protein recruitment plots shown throughout this study were divided into
1113 three phases, recruitment, fast turnover, and slow turnover, in order to study their kinetics. Entry and exit
1114 points for these phases was determined by plotting the first derivative value (i.e., velocity) of protein
1115 recruitment for each timepoint. Start of recruitment was defined as 20 seconds after velocity began to
1116 increase (t=160s, dark green), since this timepoint was more consistently associated with recruitment

1117 across events than the preceding timepoint (t=140s). End of recruitment was defined as the timepoint
1118 immediately prior to when velocity is at its minimum, or 20 seconds prior to Vmin (t=240s, light green).
1119 Start of fast turnover was defined as the timepoint associated with Vmin (t=260s, dark gray), and the end
1120 of fast turnover was defined as the point in which turnover ceased to decelerate (t=340s, light gray). Start
1121 of slow turnover was defined as the timepoint immediately following the end of fast turnover (t=360s,
1122 dark orange), and terminated at the timepoint prior to when velocity crosses the x-intercept (t=760s, light
1123 orange). This analysis was conducted for all events independently and was used as the basis for linear
1124 regression analysis to determine the rate (slope) of recruitment, fast turnover, and slow turnover across
1125 multiple proteins, strains, and inhibitor treatment conditions.
1126
1127 **Figure S3: Linear regression analysis of population-level kinetics derived from effector deletion strains.**
1128 All protein recruitment events used to generate the averaged plots shown throughout the study (Fig. 1B,
1129 Fig. 2B, Fig. 3B) were individually divided into recruitment and turnover phases (Fig. S2). Fold recruitment
1130 values were averaged for each timepoint and analyzed by linear regression to ascertain the population-
1131 level kinetics of recruitment and turnover for each condition. Averaged rate slopes were divided according
1132 to the dataset they correspond to, summarizing the rate distributions depicted as violin plots throughout
1133 the study into comprehensive linear slopes which represent the rate of protein recruitment and turnover.
1134 Statistical significance was determined by t-test, * $P \leq 0.05$, ** $P \leq 0.01$, *** $P \leq 0.001$.
1135
1136 **Figure S4: Actin turnover duration is reduced following deletion of TarP and TmeA.**
1137 Actin turnover velocity of (A) wild-type, (B,C) cis-complemented (*cis*-TarP, *cis*-TmeA), (D,E) single-
1138 knockout (ΔTarP, ΔTmeA), or (F) double-knockout (ΔTmeA/ΔTarP) *Chlamydia* strains were plotted for each
1139 timepoint. T=0 represents maximal fold recruitment of actin for each strain, with the termination of actin
1140 turnover defined by the timepoint immediately before actin velocity crosses the X-intercept (yellow dot).

1141 (G) Fold recruitment values were plotted against time for each strain, highlighting the timepoint denoting
1142 the end of actin turnover for each strain. Protein turnover duration was quantified for each recruitment
1143 event monitored across all strains and proteins utilized throughout the study.
1144
1145 **Figure S5: SMIFH2 does not inhibit myosin superfamily proteins at relatively low concentrations.**
1146 Cos7 cells were treated with (A) the nonmuscle myosin II inhibitor s-nitro blebbistatin, (B) the rho-
1147 associated protein kinase (ROCK) inhibitor Y27632, or (C) the pan-formin inhibitor SMIFH2 at various
1148 concentrations for 1 hour. Cells were probed with anti-vinculin and anti-paxillin antibodies and stained
1149 using fluorescent secondary antibodies to identify the integrity of focal adhesions following inhibitor
1150 treatment. (D) Cos7 cells were treated with blebbistatin, Y27632, or SMIFH2 at various concentrations for
1151 1 hour prior to lysis in Laemmli buffer. Lysates were resolved by SDS-PAGE followed by Western blotting
1152 and probed with antibodies reactive against phospho-myosin light chain 2 (p-MLC2 Thr18/Ser19), total
1153 myosin light chain 2 (t-MLC2), and GAPDH. (E) p-MLC2 abundance was quantified for each sample by
1154 ratiometric analysis of p-MLC2 intensity versus total MLC2 intensity, with each condition normalized
1155 against mock treatment. The concentration of SMIFH2 utilized to inhibit formins throughout this study
1156 (10µM) did not prevent the formation of intact focal adhesions or restrict phosphorylation of MLC2.
1157
1158 **Figure S6: Linear regression analysis of population-level kinetics following inhibition of formin or**
1159 **Arp2/3.**
1160 All protein recruitment events used to generate the averaged plots shown throughout the study (Fig. 4C,
1161 Fig. 5A,B,D) were individually divided into recruitment and turnover phases (Fig. S2). Fold recruitment
1162 values were averaged for each timepoint and analyzed by linear regression to ascertain the population-
1163 level kinetics of recruitment and turnover for each condition. Averaged rate slopes were divided according
1164 to the dataset they correspond to, summarizing the rate distributions depicted as violin plots throughout

1165 the study into comprehensive linear slopes which represent the rate of protein recruitment and turnover.

1166 Statistical significance was determined by t-test, * P ≤ 0.05, ** P ≤ 0.01, *** P ≤ 0.001.

1167

1168 **Figure S7: Kinetics of mDia1 and mDia2 recruitment and turnover are attenuated by Arp2/3 inhibition.**

1169 All mDia1/2 recruitment events used to create the averaged plot shown previously (Fig. 2D) were

1170 individually divided into recruitment, fast turnover and slow turnover phases (Fig. S2). (D) Individual rates

1171 of recruitment were plotted on a violin plot with inset boxplot, reporting the median rate +/- SD for each

1172 inhibitor treatment condition. (E) Individual rates of fast turnover (Left) and slow turnover (Right) were

1173 plotted using the same method as recruitment, with fast and slow turnover plots grouped together

1174 according to condition. Violin plots contain a minimum N=22 individual rates. Statistical significance was

1175 determined by Wilcoxon Rank-sum. Data are representative of at least 3 independent experiments, ** P

1176 ≤ 0.01, *** P ≤ 0.001.

1177

1178 **Table S1: Statistical values associated with recruitment and turnover of actin following effector**
1179 **deletion**

1180 **Table S2: Statistical values associated with recruitment and turnover of Arp3 following effector**
1181 **deletion**

1182 **Table S3: Statistical values associated with recruitment and turnover of formin 1 following effector**
1183 **deletion**

1184 **Table S4: Statistical values associated with recruitment and turnover of actin following inhibitor**
1185 **treatment**

1186 **Table S5: Statistical values associated with recruitment and turnover of formin 1 and Arp3 following**
1187 **inhibitor treatment**

1188 **Table S6: Statistical values associated with recruitment and turnover of mDia1/2 in presence and**
1189 **absence of CK666**

1190 **Table S7: Pairwise correlation analyses of mDia1/2 kinetics in presence and absence of CK666**

1191 **Video S1: Representative video of fluorescent protein recruitment during *Chlamydia* invasion**

1192 Cos7 cells were transfected with plasmids expressing various GFP-fusion proteins for 24 hours prior to
1193 infection with CMTPX-stained *C. trachomatis* EBs (MOI=20). Bacterial adhesion and entry was monitored
1194 by live-cell imaging using a spinning disk confocal microscope (Nikon CSU-W1 or Leica SD6000 AF),
1195 obtaining images every 20 seconds for 30 minutes to identify sites exhibiting protein recruitment. Images
1196 were assembled into videos in ImageJ and annotated to highlight recruitment events. The representative
1197 video shown here depicts GFP-actin recruitment at sites where CMTPX-*Chlamydia* contacts the host cell
1198 (arrows). Similar videos were assembled for all proteins monitored throughout the study, each yielding
1199 recruitment events that exhibit tight localization around fluorescent *Chlamydia*, enabling straightforward
1200 quantification of recruitment intensity and duration (Figs. S1-3).
1201
1202 **Video S2: Co-inhibition of formin and Arp2/3 yields abnormal actin recruitment kinetics around**
1203 **invading *Chlamydia***
1204 Cos7 cells were transfected with GFP-actin 24hrs prior to pretreatment with 10µM SMIFH2 and 100µM
1205 CK666 for 1hr. Transfected cells were infected with unlabeled *Chlamydia* at MOI=20 and imaged by
1206 quantitative live-cell imaging, collecting images every 20 seconds for 30 minutes. Images were assembled
1207 into videos in ImageJ and annotated to highlight recruitment events (arrows).

Figure 1

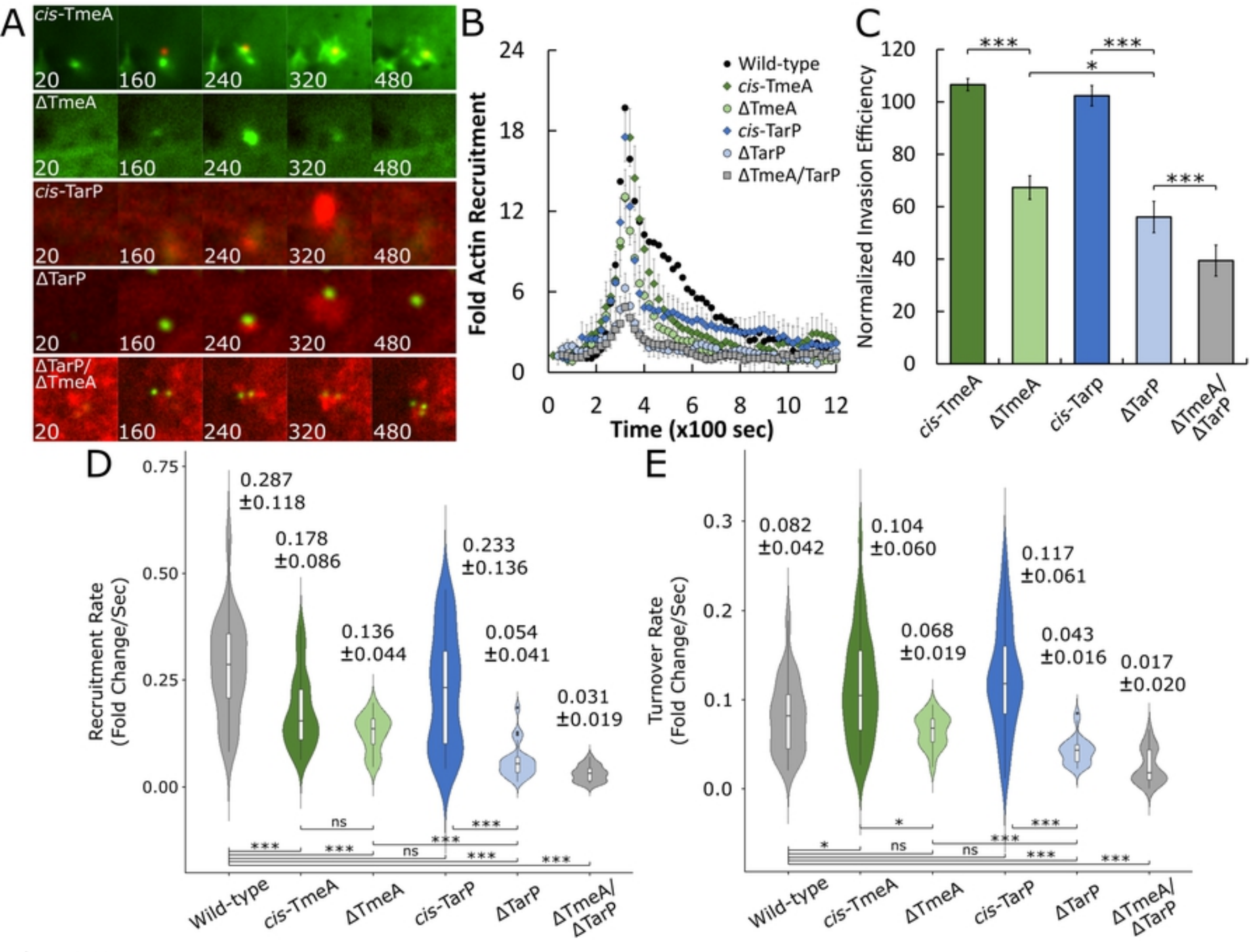

Figure 1

Figure 2

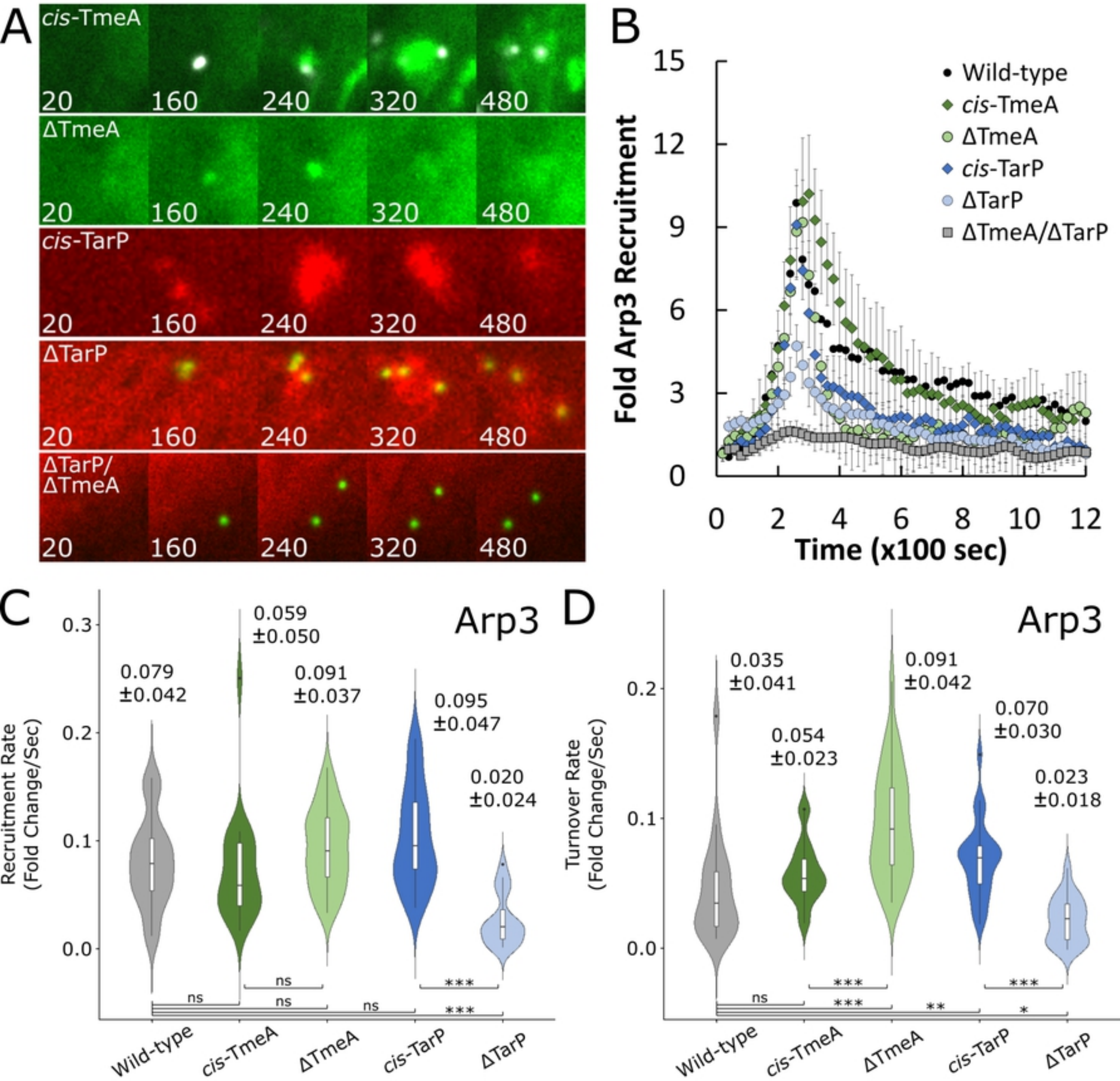

Figure 2

Figure 3

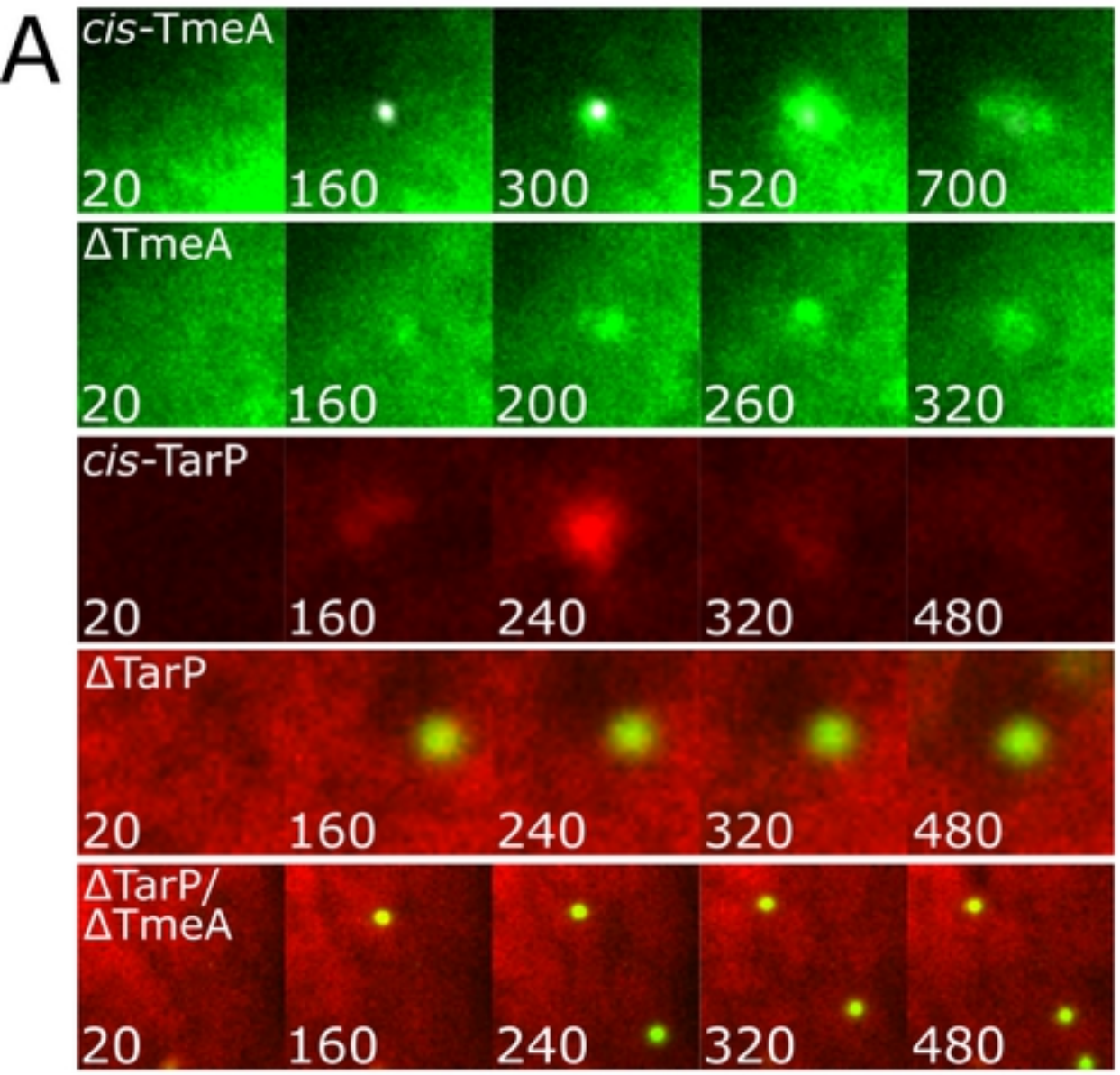

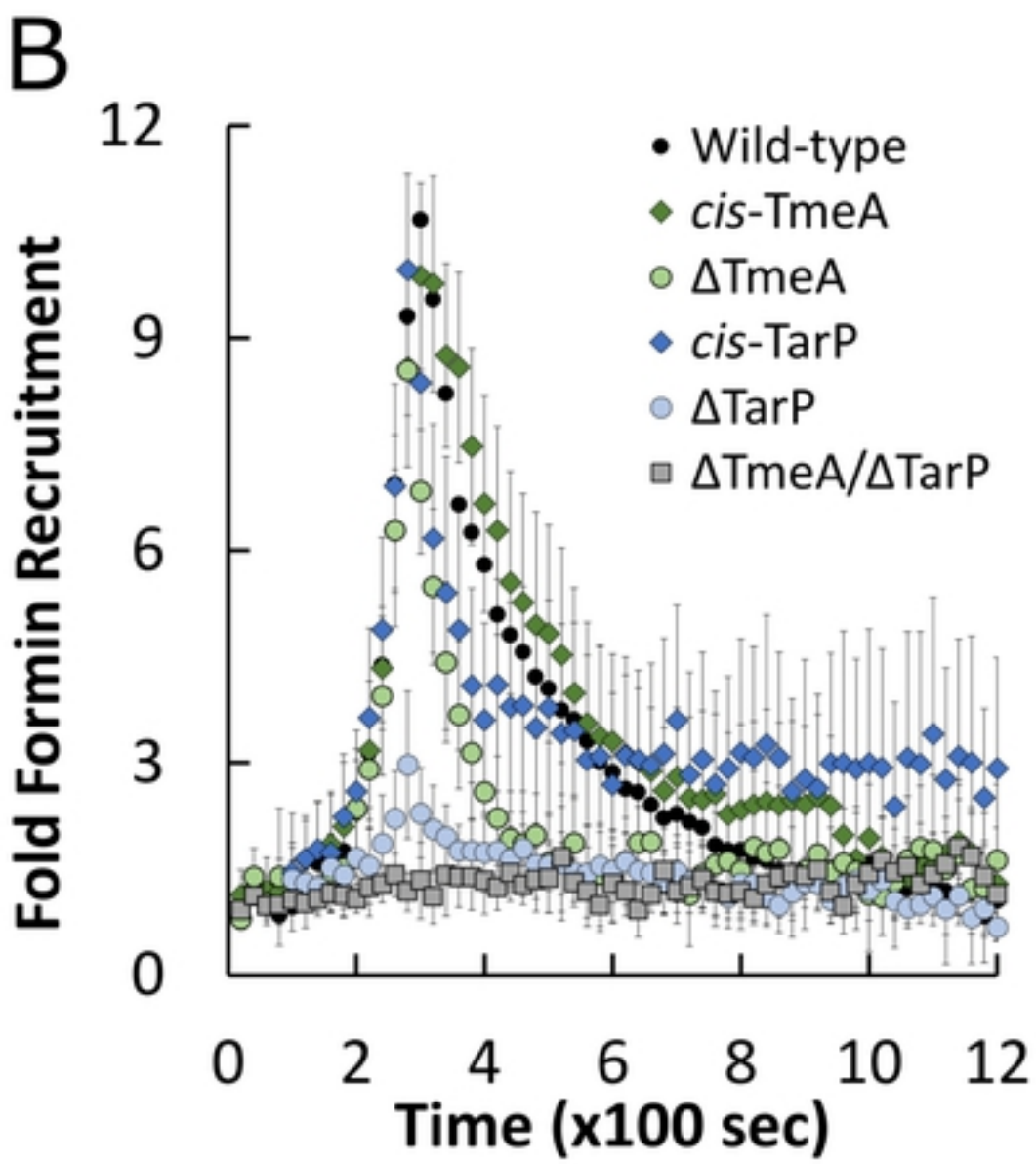

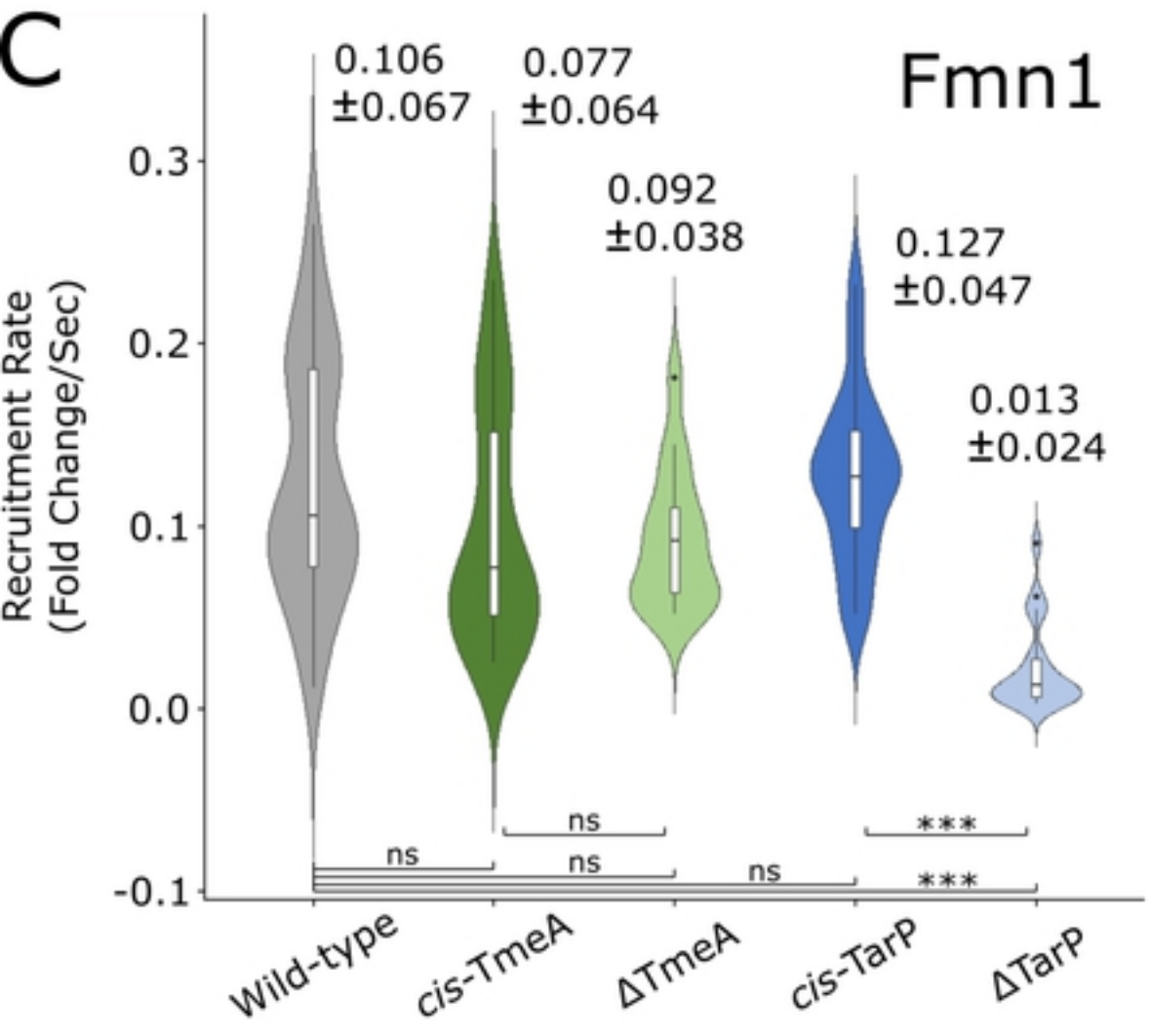

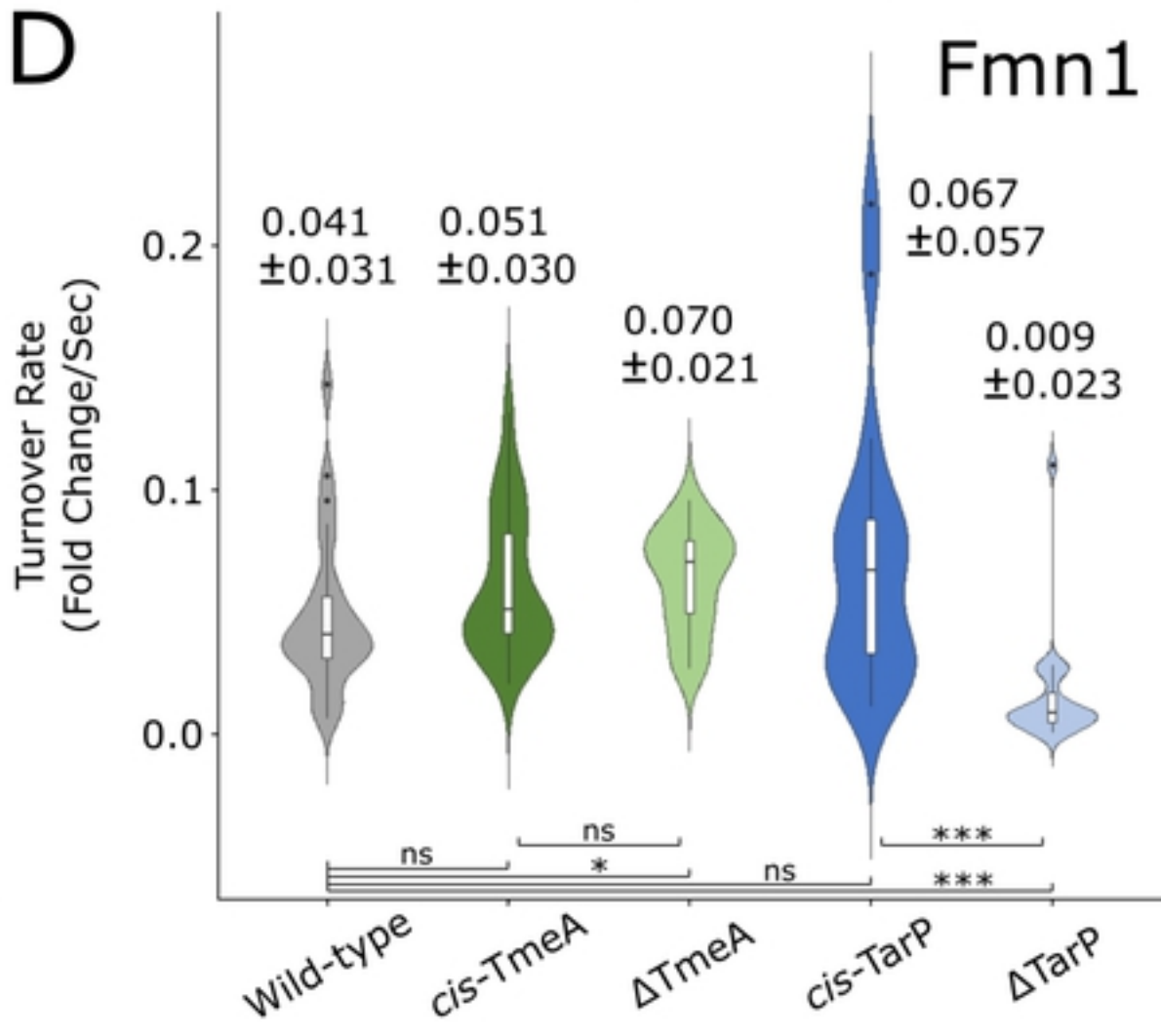

Figure 3

Figure 4

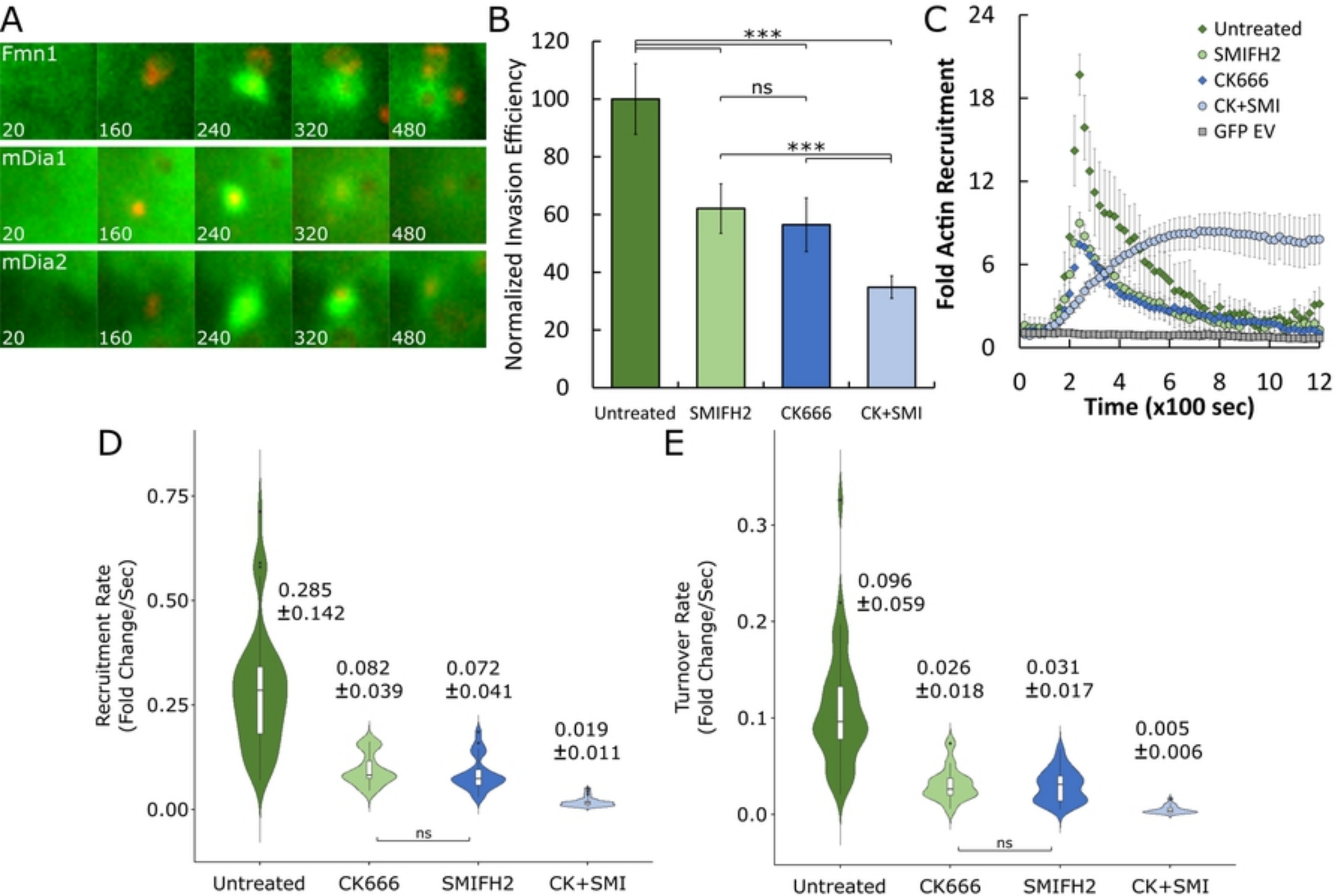

Figure 4

Figure 5

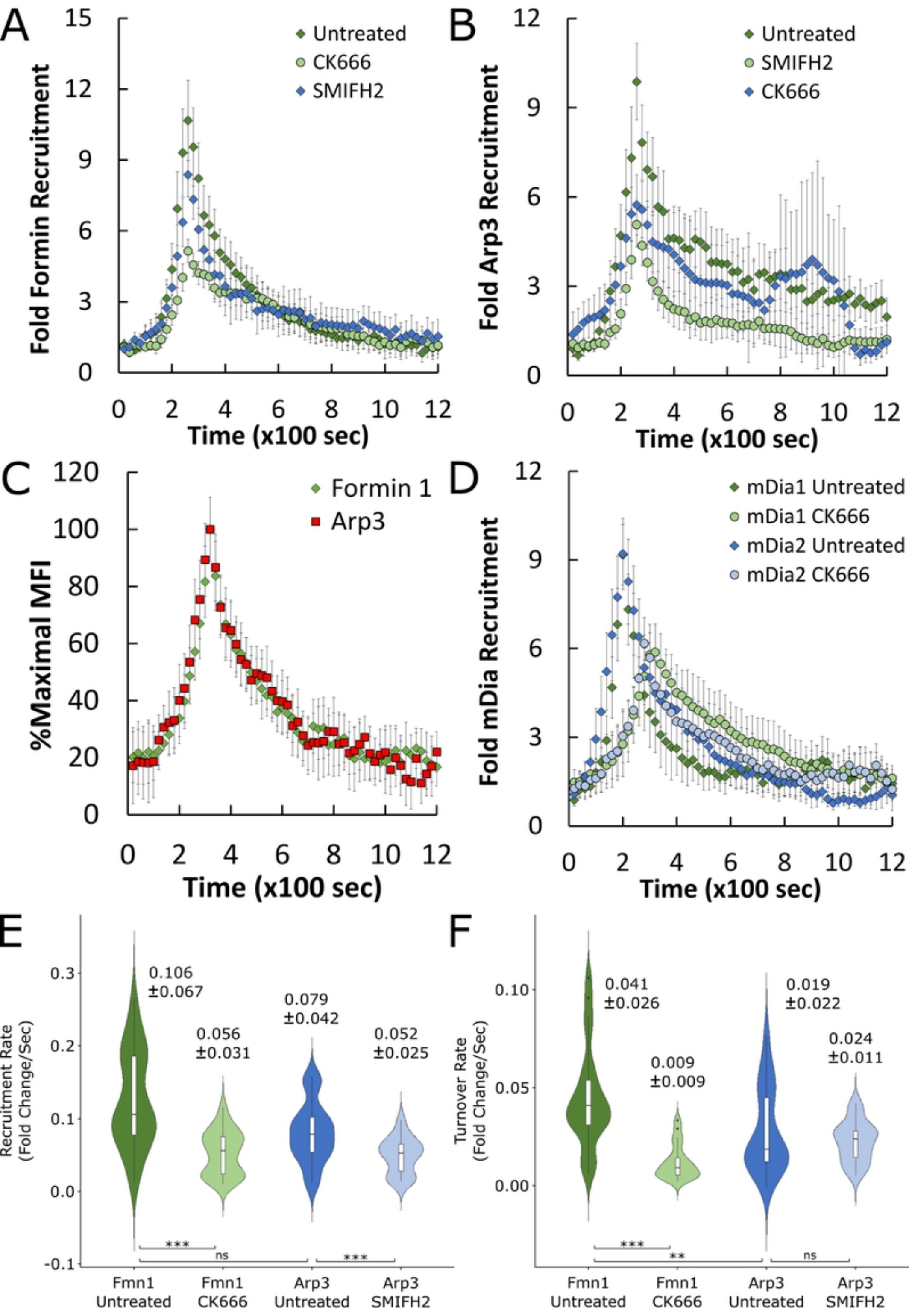

Figure 5

Figure 6

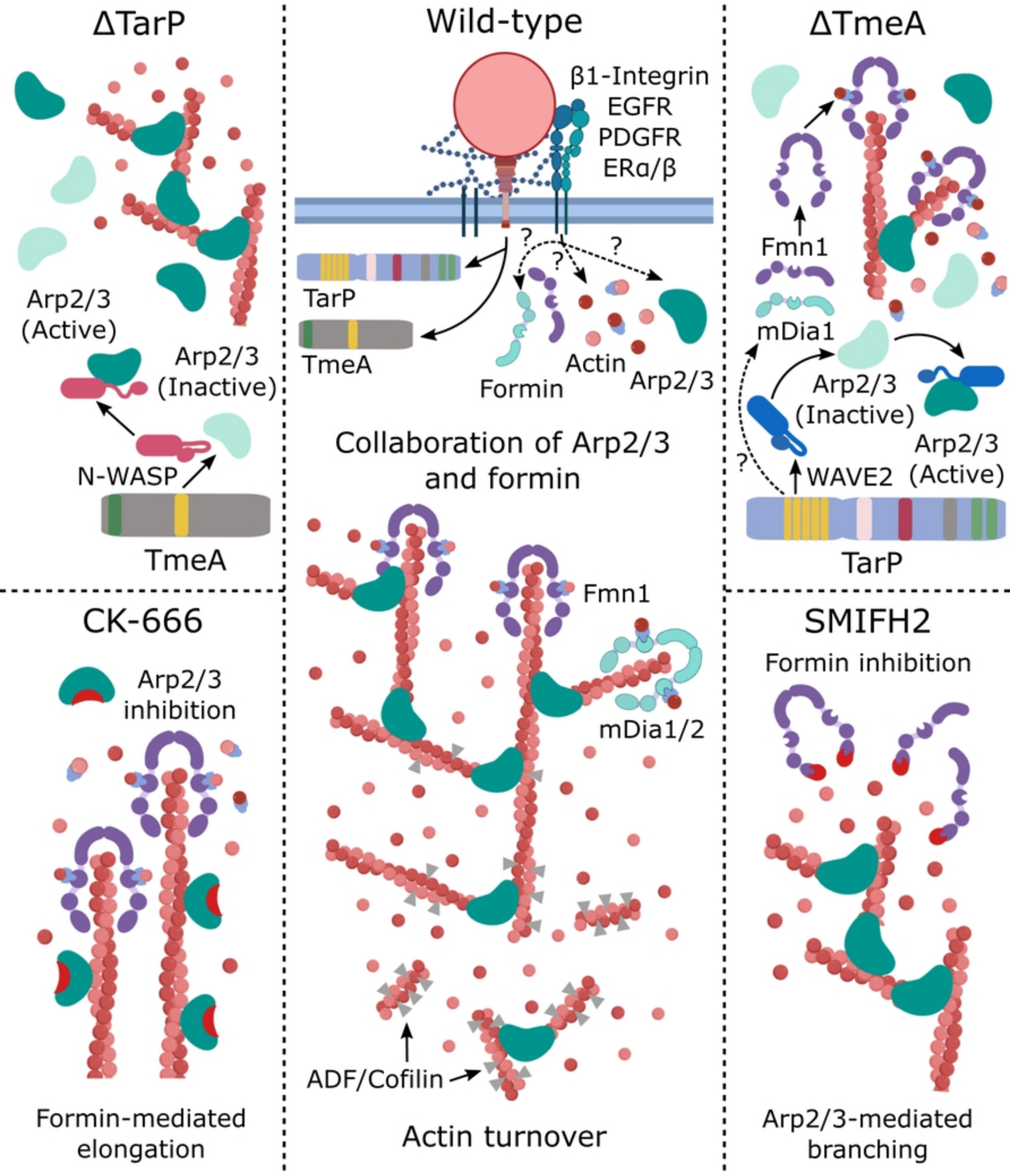

Figure 6